



**Sudan University of Science and Technology**



**College of Graduate Studies**

**Preparation, Characterization and Application of Zinc Oxide and  
Nickel Doped Zinc Oxide Nanoparticles at High Temperature**

**تحضير وتوصيف واستخدام اكسيد الزنك واكسيد الزنك النانوى المشوب بالنيكل فى درجة  
حرارة عالية**

**A Dissertation Submitted in Partial Fulfillment of the Requirement of the Degree of Master  
of Science in Chemistry**

**By**

**Mohamed Yousif Elhaj Mohamed (Bsc Honors Chemistry)**

**Supervisor: Dr. Elfatih Ahmed Hassan**

**2020**

## إستهلال

بسم الله الرحمن الرحيم

قال تعالى:

﴿لَقَدْ أَرْسَلْنَا رُسُلَنَا بِالْبَيِّنَاتِ وَأَنْزَلْنَا مَعَهُمُ الْكِتَابَ وَالْمِيزَانَ لِيَقُومَ النَّاسُ بِالْقِسْطِ ۗ وَأَنْزَلْنَا الْحَدِيدَ فِيهِ بَأْسٌ شَدِيدٌ وَمَنَافِعُ لِلنَّاسِ وَلِيَعْلَمَ اللَّهُ مَن يَنْصُرُهُ وَرُسُلَهُ بِالْغَيْبِ ۗ إِنَّ اللَّهَ قَوِيٌّ عَزِيزٌ﴾

(سورة الحديد الآية 25)

# **Dedication**

To my

Parent, Brothers and Sisters

## **Acknowledgements**

Praise to Allah, Almighty, Who gave me Health, Strength and patience to conduct this research.

I would like to express my deep gratitude and indebtedness to my supervisor **Dr. Elfatih Ahmed Hassan** for his keen guidance and advice throughout this study.

I am very grateful to **Dr. Abueliz Khalid Modwi** for Technical support.

Finally, sincere thanks go to my colleagues and friends in Sudan University of Science and Technology, and to all, those who helped and inspired me during my work for their moral support.

## Abstract

Pure Zinc oxide and nickel doped zinc oxide nanoparticles were prepared by precipitation method at high temperature (700C°).

The Shape and size of these prepared nanostructures were then characterized by UV absorption, SEM, and FTIR technique. Band gap of ZnO and Ni/ ZnO were calculated from UV absorption measurement and it was found to be 3.9eV and 3.85eV respectively.

Scanning electron microscopy measurement showed that the average particle size of ZnO and Ni/ ZnO were 62.5 and 83.1nm respectively

FTIR confirmed the formation of ZnO as evident from stretching frequency band for Zn-O at  $446.3\text{cm}^{-1}$ , which was shifted to  $438.5\text{cm}^{-1}$  for doped Ni-ZnO.

FTIR spectrum, provide supportive evidence for successful formation of Zinc oxide and nickel doped zinc oxide.

The rate constant for catalytic photo degradation of methyl orange was calculate for two nano catalyst used and was found to be  $0.0185\text{min}^{-1}$  and  $0.0225\text{min}^{-1}$  for zinc oxide and nickel doped zinc oxide respectively.

Percentage degradation after 110 minute was 60% and 71% for ZnO and Ni/ ZnO respectively.

## المستخلص

تم تحضير اكسيد الزنك النقى واكسيد الزنك النانوى المشوب بالنيكل باستخدام طريقة الترسيب فى درجه حراره عاليه 700 درجه مئوية .

تم توصيف شكل وحجم الجسيمات النانويه المحضرة باستخدام تقنية امتصاص الاشعه فوق البنفسجيه ؛ ومسح المجهر الالكترونى ، وتقنية الاشعة تحت الحمراء. تم حساب طاقة الفجوة بالنسبة لأكسيد الزنك واكسيد الزنك النانوى المشوب بالنيكل من قياس الاشعة فوق البنفسجية ووجدت ان قيمتها تساوى 3.9 و 3.85 الكترون فولت على التوالى.

اظهرت قياسات المسح المجهرى الالكترونى ان متوسط حجم الجسيمات النانوية لكل من من اكسيد الزنك واكسيد الزنك النانوى المشوب بالنيكل هي 62.5 و 83.1 نانومتر على التوالى.

اكنت دراسة الاشعة فوق الحمراء تكون اكسيد الزنك النانوى الذى دل عليه ظهور حزمه تردد استطالة رابطه Zn-O عند التردد 446.3 سم<sup>-1</sup> ، والذى تمت ازاحتة الى التردد 438.5 سم<sup>-1</sup> .

دراسة طيف الاشعة تحت الحمراء يوفر دليلا داعما لنجاح تكون اكسيد الزنك واكسيد الزنك النانوى المشوب بالنيكل.

تم حساب ثابت سرعة تفاعل التحلل الضوى للمثيل البرتقالى باستخدام كل من الحفازين النانوين اكسيد الزنك واكسيد الزنك النانوى المشوب بالنيكل ووجد ان قيمة كانت 0.0185 دقيقه<sup>-1</sup> و 0.0225 دقيقه<sup>-1</sup> لكل منهما بالترتيب.

نسبة التحلل بعد 110 دقيقة كانت 60% و 71% لكل من اكسيد الزنك واكسيد الزنك النانوى المشوب بالنيكل على التوالى

## Table of Contents

No.	Topic	Page
	استهلال	VI
	Dedication	VI
	Acknowledgements	VI
	Abstract	VI
	المستخلص	VI
	Table of Contents	VI
	List of Tables	VI
	List of Figures	VI
	List of Abbreviation	VI
	<b>Chapter One</b> <b>Introduction and literature Review</b>	
1.1	Nanotechnology	1
1.2	Classification of Nanoparticles	2
1.2.1	One Dimension Nanoparticles	2
1.2.2	Two Dimension Nanoparticles	2
1.2.3	Three Dimension Nanoparticles	3
1.3	Preparation Conditions of Nanostructure	4
1.4	Metal Oxides	4
1.5	Synthesis Techniques of Nanoparticles (top-down and bottom up)	5
1.6	Zinc Oxide Nanostructures-Synthesis Methods	6
1.7	Preparation of Nanoparticles	7
1.7.1	Hydrothermal Growth	7
1.7.2	Milling Process	8
1.7.3	Chemical Bath Deposition	10
1.8	Crystal Structure of ZnO	10
1.9	ZnO Nanoparticles Structure	11
1.10	Characterization of Zinc Oxide Nanoparticles	16
1.10.1	X-ray Diffraction Analysis	16
1.10.2	Transmission Electron Microscopy	17
1.10.3	FTIR Spectroscopy	18
1.10.4	UV-Visible Spectroscopy	19

1.10.5	DSC Analysis	21
1.11	Literature Review	22
1.12	Objectives Of The Study	27
	<b>Chapter Two Material And Methods</b>	
2.1	Material	28
2.1.1	Chemicals	28
2.2	Apparatus	29
2.3	Instruments	29
2.4	Method	29
2.4.1	Synthesis of ZnO	29
2.4.2	Synthesis of 5% Ni doped ZnO	30
2.4.3	Scanning Electron Microscope Measurement(SEM)	30
2.4.4	Fourier Transform Spectroscopy Measurement (FTIR)	31
2.4.5	UV. Measurement	31
2.4.6	Methyl Orange Degradation Kinetic	32
	<b>Chapter Three Results and Discussion</b>	
3.1	Characterization of ZnO and Ni/ZnO nanoparticles	34
3.1.1	Scanning Electron Microscopy (SEM)	34
3.1.2	Fourier Transforms Infrared Studies (FTIR)	36
3.2	Estimation Of Band gab in ZnO and Ni /ZnO	37
3.3	Photo Catalytic Performance	40
3.3.1	Kinetic Adsorption of methyl orange	40
3.3.2	Catalytic Degradation	43
3.4	Conclusions	44
	References	45

## List of Tables

<b>Table No</b>	<b>Topic</b>	<b>Page</b>
(1.1)	Morphologies obtained using different templates. Particle	7
(3.1)	Adsorption Kinetic Data for Methyl Orange Using ZnO	40
(3.2)	Kinetic Adsorption Data for Methyl Orange Using Ni/ZnO	40

## List of Figures

Figure No	Topic	Page
(1.1)	The Hexagonal Wurtzite Structure Model of ZnO.	11
(1.2)	TEM Micrographs of ZnO Nanoparticles.	13
(1.3)	XRD Patterns of ZnO Nanoparticle	16
(1.4)	TEM Images of ZnO Nanoparticles (a, b) and its selected area electron Diffraction Image (c).	17
(1.5)	FTIR Spectra of ZnO Nanoparticles	18
(1.6) (a)	Absorption of ZnO Nanoparticles as a Function of Wavelength	19
(1.6) (b)	Variation of $(\alpha h\nu)^2$ with $h\nu$ for ZnO nanoparticles as a function of wavelength at $1/2 n$ value	20
(1.7)	DSC Curve of ZnO Nanoparticles	21
(1.8)	Worldwide Consumption of Zinc Oxide.	22
(1.9)	Schematic Representation The Application of ZnO.	22
(2.1)	Scanning Electron Microscope SEM Energy Disperse X-ray EDX (JEOL 7000f)	30
(2.2)	Fourier Transforms Infrared Spectroscopy FTIR-8400S	31
(2.3)	Photoluminescence Analyzer PL (Perkin Elmer LS55 luminescence)	32
(2.4)	Spectrophotometer (Labomed – UVS-2800)	33
(3.1)	SEM Images of pure ZnO	34
(3.2)	SEM Images of Ni <sub>5%</sub> doped ZnO	35
(3.3)	SEM Images of pure ZnO With Particle Size	34
(3.4)	Ni <sub>5%</sub> doped ZnO Nanoparticles With Particle Size	36
(3.5)	Fourier Transforms Infrared for ZnO and Ni /ZnO	37
(3.6)	Undoped ZnO at 700 C°	38
(3.7)	Ni doped ZnO at 700 C°	38
(3.8)	band gap of pure ZnO	39
(3.9)	band gap of Ni/ZnO	39
(3.10)	Absorbance VS Time (ZnO)	41
(3.11)	$\ln C_0/C_t$ VS Time (ZnO)	41
(3.12)	Absorbance VS Time (Ni/ZnO)	42
(3.13)	$\ln C_0/C_t$ VS Time (Ni/ZnO)	42

## List of Abbreviation

<b>Abbreviation</b>	<b>Explanation</b>	<b>Page</b>
CNTs	Carbon Nanotubes	2
SWCNTs	Single Walled Carbon Nanotubes	2
MWCNTs	Multi Walled Carbon Nanotubes	2
ID	One Dimension	3
NBE	Near Band Emission	4
ZNRAs	Zinc Oxide Nanorods Arrays	4
ZAH	Zinc Acetate Hydrate	6
TMAH	Tetra Methyl Ammonium Hydroxide	6
MOCVD	Metal Organic Chemical Vapour Deposition	6
VS	Vapour Solid	6
VLS	Vapour Liquid Solid	6
MTS	Mechanical Thermal Synthesis	9
XRD	X-ray Diffraction	9
SEM	Scanning Electron Microscopic	9
LEDs	White Light Diodes	10
THF	Tetrahydrofuron	12
TEM	Transmission Electron Microscopic	12
HAD	Hexadecylamine	12
DDA	Dodecylamine	13
OA	Octylamine	13
FETEM	Field Emission Electron Microscopy	14
IPCE	Incident Photon To Electron Conversion Efficiency	16
SAED	Selected Area Electron Diffraction	17
DSC	Differential scanning calorimetry	21
ITO	Indium Tin Oxide	23
TCO	Transparent Conducting Oxide	23
NRs	Nanorods	23
NPs	Nanoparticles	23
IEP	Isoelectric Point	23
ChOx	Cholesterol Oxidase	24
PPDME	Protoporphyrin Dimethyl Ester	24
NCs	Nanocorals	25
POF	Poly 9.9-Di Octyl Fluorene	26
EL	Electroluminescence	26
CCT	Correlated Color Temperature	26
CRI	Color Rendering Index	26
PL	Photoluminescence	31
FTIR	Fourier Transforms Infrared	35

# Chapter One

## Introduction

### 1.1 Nanotechnology?

The prefix Nano has found in last decade, an ever- increasing application to different fields of knowledge. Nanoscience, Nanotechnology, Nonmaterial's are only a few of the new Nano-containing, terms in scientific reports, in popular books as well as in newspapers and that have become familiar to a wide public, even of non-experts. The prefix comes from the ancient Greek  $\nu\alpha\nu$  through the Latin nanus meaning literally dwarf and, by extension, very small. Within the convention of International System of Units (SI) it is used to indicate a reduction factor of  $10^9$  times. So, the nanosized world is typically measured in nanometers (1nm corresponding to  $10^{-9}$  m) and it encompasses systems whose size is above molecular dimensions and below macroscopic ones (generally larger than 1nm and below 100 nm) (Dupas, C. et al, 2007)

Nanotechnology is use and manipulation of matter at a tiny scale. At this size, atoms and molecules work differently, and provide a variety of surprising and interesting uses.( Reddy et al, 2010)

Nanotechnology and Nanoscience studies have emerged rapidly during the past years in a broad range of product domains. It provides opportunities for the development of materials, including those for medical applications, (Roco et al, 2011)

Where conventional techniques may reach their limits. Nanotechnology should not be viewed as a single technique that only affects specific areas. Although often referred to as the 'tiny science', nanotechnology does not simply mean very small structures and products. Nanoscale features are repeatedly incorporated into bulk materials and large surfaces. Nanotechnology represents the design, production and application of materials at atomic, molecular and macromolecular scales, in order to produce new nanosized materials. Pharmaceutical nanoparticles are defined as solid, submicron-sized (less than 100 nm in diameter) drug carrier that may or may not be biodegradable.( Pal et al, 2011)

The term nanoparticle is a combined name for both nanospheres and nanocapsules. Nanospheres are matrix system in which drug is uniformly dispersed, while nanocapsules are the system in which the drug is surrounded by a unique polymeric membrane.( Tiruwa et al, 2016)

This systemic review focuses on Classification, method of Preparation, Characterization, and Application, health prospective and Pharmacological aspects of nanoparticles.

In recent years the research on nanostructures of different materials and their use for devices and systems have been increasing. The reason for this is the unique properties of nanostructures that are advantageous over bulk materials. An example of this is the dependence of the chemical and physical properties of nanostructures on size. For example the relatively large surface area to volume ratio renders surface effects and forces to dominate over other forces.( Koch et al,2009)

Such property would lead to potential use of some nanomaterials for many applications, like e.g. for sensors. Adding to this the order of size of nanostructures which is similar to many biological analytes and chemical species would render their sensitivity to be quite high even in small volumes. The intensified research on growth and prototype devices based on nanostructures has reached a stage where reproducibility and control of the nanostructures is acceptable for many materials. Many materials are under focus with the potential of developing nano -systems. The optimization of the performance is the main challenge at the moment. (Jiang et al, 2011)

## **1.2 Classification of Nanoparticles**

There are various approaches for classification of nonmaterials. Nanoparticles are classified based on their dimensions

### **1.2.1 One Dimension Nanoparticles**

One dimensional system, such as thin film or manufactured surfaces, has been used for decades in electronics, chemistry and engineering. Production of thin films (sizes1-100nm) or monolayer is now common place in the field of solar cells or catalysis. These thin films are used in different technological applications, including information storage systems, chemical and biological sensors, fibre-optic systems, magneto-optic and optical device.( Ali et al,2016)

### **1.2.2 Two Dimension Nanoparticles**

#### **Carbon nanotubes (CNTs)**

Carbon nanotubes are hexagonal network of carbon atoms, 1 nm in diameter and 100 nm in length, as a layer of graphite rolled up into cylinder. CNTs are of two types, single walled carbon nanotubes (SWCNTs) and multi-walled carbon nanotubes (MWCNTs) .The small dimensions of carbon nanotubes combined with their remarkable physical, mechanical and electrical properties, make them unique materials. They display metallic or semi conductive properties, depending on

the carbon leaf is wound on itself. The current density that nanotubes can carry is extreme and can reach one billion amperes per square meter making it a superconductor. The mechanical strength of carbon nanotubes is sixty times greater than the best steels. Carbon nanotubes have a great capacity for molecular absorption and offering a three dimensional configuration. Moreover they are chemically very stable.( Eatemadi et al,2014)

### **1.2.3 Three Dimension Nanoparticles**

#### **Fullerenes (Carbon 60)**

Fullerenes are spherical cages containing from 28 to more than 100 carbon atoms, contain C<sub>60</sub>. This is a hollow ball composed of interconnected carbon pentagons and hexagons, resembling a soccer ball. Fullerenes are class of materials displaying unique physical properties. They can be subjected to extreme pressure and regain their original shape when the pressure is released. These molecules do not combine with each other, thus giving them major potential for application as lubricants. They have interesting electrical properties and it has been suggested to use them in the electronic field, ranging from data storage to production of solar cells. Fullerenes are offering potential application in the rich area of Nano electronics. Since fullerenes are empty structures with dimensions similar to several biological active molecules, they can be filled with different substances and find potential medical application (Pal et al (2011)).

One-dimensional (1D) semiconductors have attracted enormous attention in recent decades not only for fundamental physical and chemical studies but also for promising applications in various technological areas. Huge scientific efforts have been devoted toward fabricating (1D) nanostructures. Zinc oxide (ZnO) is an II-VI semiconductor material with many interesting properties such as a wide band gap of about 3.37 eV and exciton binding energy of 60 meV both at room temperature. In addition, ZnO provides laser action at room temperature due to electron-hole plasma. This is along with a high piezoelectric tensor owing to the high ionicity nature of the Zn-O bond. Preferentially, ZnO crystallizes in a hexagonal wurtzite crystal structure, space group P6<sub>3</sub> mc or C<sub>6v</sub>. Other crystal structures phases such as rock-salt and zinc-blend are also present metastable crystal forms of ZnO. Among all the attractive properties of ZnO, the excellent optical properties are paving the way for a diversity of optoelectronics applications including white light emitting diodes and field emission devices, despite the fact that a reliable and stable p-type doping essential for p-n junction necessary for electronic and optoelectronic applications is

difficult to accomplish.( Li et al,2012)

ZnO nanostructured materials such as nanorods, nanowires, and nanotubes grow mainly along the c-axis of the hexagonal wurtzite crystal structure of ZnO and have recently been reported.(Wang et al,2004)

On the other hand, nanobelts, nanosprings, and nanohelices have also been demonstrated, and they represent the family of ZnO nanostructures growing along the a-axis.( Wang et al,2009)

### **1.3 Preparation Conditions of Nanostructure**

The growth of these nanostructures has been performed in two temperature regimes. These are the low temperature wet chemical techniques at temperatures as low as 100 °C and high temperature physical or physio-chemical strategies at temperatures higher than 600°C Both strategies have advantages and disadvantages. For instance, the chemical bath deposition as an example of a wet chemical technique yields a simple two-step growth procedure for well- aligned, ZnO nanorods, but shows a large presence of defects associated with the photoluminescence of the as-grown samples. A post annealing is essential for obtaining a better near band emission (NBE) for such grown ZnO nanorods arrays (ZNRAs). High temperature growth techniques on the other hand require complex equipment and in many circumstances cannot be utilized for large area deposition. In addition, high temperature techniques cannot be achieved using certain types of substrates, for example, flexible plastic substrates (Zainelabdin A. et al, 2010)

### **1.4 Why is metal oxides?**

Among all the functional materials designed at the nanoscale, metal oxides and mixed metal oxides are, particularly, attractive candidates from a scientific as well as technological point of view. The unique characteristics of metal oxides structured at the nanoscale make them the most diverse class of materials, with properties covering almost all of the aspects of materials science and solid state physics.

Nanoscale metal oxides play an important role in the different fields of nanoscience and nanotechnology, e.g., biology, chemistry, physics, materials science, from electronics to nanomedicine. The preparation of metal oxide nanocrystals can be achieved through many different approaches by either physical or chemical methods. Among them, the surfactant-assisted pathways are the most easily controlled for the size, shape, composition, and phase structure of the resulting nanocrystals.( Koziej et al,2014)

The importance of the surfactant is highlighted by the fact that nanocrystals produced by colloidal

routes are generally considered together with the surfactants that coat them. This organic coating allows additional synthetic flexibility in which the surfactants can be substituted different organic molecules with different functional groups or polarity. (Baghbanzadeh et al,2011)

Although there have been many new interesting developments in the shape control of metal oxide nanocrystals in the past few years, (Jun et al,2006)

there is still a great deal of work to be done. Current shape control strategies still highly on experimental trial-and-error approaches rather than on rational design of synthetic strategies. The next step should focus on the development of more versatile and reliable but simple synthetic schemes tailored for architecture of nanocrystals with desired components. Concurrently, a better understanding of the guiding principles of crystal growth at the nanoscale level should be pursued. This knowledge will enable further fine tuning of the size, shape, and surfaces, and thus functionalities, of nanocrystals. Additionally, the synthesis of hybrid nanocrystals in which nanocrystals of different shapes and properties are connected together in a single particle is also a fascinating subject. The success in synthesizing such multi-component nanocrystals will open access to a completely novel generation of colloidal structures with prospects of optoelectronic, magnetic, biomedical, photovoltaic, and catalytic applications with high level of performance. (Goodman et al,2017)

Metal oxide nanocrystals in a variety of shapes such as spheres, cubes, rods, wire, disks, and polypods

## **1.5 Synthesis Techniques of Nanoparticles (top-down and bottom up)**

The syntheses of nanoparticles are generally grouped into two broad categories: -  
"bottom up" and "top down" (Anderson et al,2018)

The process in which materials prepared from atomic precursors assemble to form clusters and subsequently nanoparticles is referred to as "bottom up" approach. Conversely, when the nanoscale is reached by physically disassembling large building blocks, the process is referred to as "top down" approach. The advantage of the physical methods is the possibility to produce a large quantity of nanoparticles, whereas synthesis and control of uniform-sized nanoparticles remain very difficult using the top-down route. (Sau et al,2010)

The "bottom up" approach is of prime interest for chemistry and materials science because the fundamental building blocks are atoms; thus colloidal chemical synthetic methods can be utilized

to prepare uniform nanocrystals with controlled particle size. using solution phase synthetic methods that enable, a proper, shape and size control of metal oxide nanocrystals, methods which include solvothermal/hydrothermal procedures, two-phase routes, microemulsions, and thermal decomposition.( Tao et al,2008)

These techniques involve the use of surfactant molecules and, consequently, result in oxide nanocrystals comprising an inorganic core coated with a layer of organic ligand molecules. This organic capping provides electronic and chemical passivation of the surface dangling bonds, prevents uncontrolled growth and agglomeration of the nanoparticles, and permits chemical manipulations of the nanoparticles similarly to large molecules having their solubility and reactivity determined by the nature of the surface ligands (Dinh et al, 2012).

### **1.6 Zinc Oxide Nanostructures-Synthesis Methods**

The synthesis methods of different zinc oxide nanostructures can broadly be classified as follows:

a. Solution phase synthesis: In this method, the growth process is carried out in a liquid. Normally aqueous solutions are used and the process is then referred to as hydrothermal growth process.

Some of the solution phase synthesis processes are:

1. Zinc Acetate Hydrate (ZAH) derived nano-colloidal sol-gel route
2. ZAH in alcoholic solutions with sodium hydroxide (NaOH) or tetra methyl ammonium hydroxide (TMAH) (Baruah et al,2009)
3. Template assisted growth
4. Spray pyrolysis for growth of thin films.
5. Lectrophoresis (Geng et al,2009)

b. Gas phase synthesis: Gas phase synthesis uses gaseous environment in closed chambers.

Normally the synthesis is carried out at high temperatures from 500 °C to 1500°C some commonly used gas phase methods are:

1. Vapour phase transport, which includes vapour solid (VS) and vapour liquid solid (VLS) growth
2. Physical vapour deposition
3. Chemical vapour deposition
4. Metalorganic chemical vapour deposition (MOCVD).

5. Thermal oxidation of pure Zn and condensation
6. Microwave assisted thermal decomposition (Loidreau et al,2011)

## 1.7 Preparation of Nanoparticles

### 1.7.1 Hydrothermal Growth

Nanoparticles. Even though the organometallic synthesis of ZnO nanoparticles in alcoholic medium has received wider acceptance for reasons of faster nucleation and growth as compared to water, still scattered reports of hydrothermal synthesis in aqueous medium are available in synthesized nanoparticles of different morphologies using ZnCl<sub>2</sub> and NaOH in a hydrothermal growth process using different organic compounds as template agents. A significant change in the morphology was observed as the synthesis temperature was increased with the particles changing from rod like to polyhedral. It was reported that the morphology also changed with the addition of different organic templates to the reaction mixture when the temperature was maintained at 160 °C. The various morphologies along with the templates used are listed in table 1.

**Table (1.1): Morphologies obtained using different templates. Particle properties**

Additive	Morphology	Size (nm)
Tributylamine	Rod-like	200–300
Trimethylamine	Rod-like	100–300
Triethanolamine	Spindle-like	100–300
Diisopropylamine	Rod-like	200–400
Ammonium phosphate	Rod-like	200–500
1, 6-Hexadecanol	Rod-like	300–700
Triethylololol	Rod-like	100–300
Isopropylamine	Rod or sheet-like	
Cyclohexylamine	Sheet-like	300–500
n-Butylamine	Sheet-like	200–400
Ammonium chloride	Sheet	50–200
Hexamethylenetetramine	Snow-flake like	20–50
Ethylene glycol	Ellipse	40–100
Ethanolamine	Polyhedron	50–200

A very simple procedure to prepare ZnO nanoparticles at a very high pH ~14 using tetramethylammonium hydroxide (TMAH) as a precipitating agent was suggested by (Baruah et al,2009)

Nanoparticles sized from 10 to 20 nm were precipitated at room temperature by adding TMAH to an ethanolic solution of zinc acetate dehydrate. Addition of water to the ethanolic solution prior to adding TMAH yielded ZnO snowflakes. Vishwanathan and Gupta have shown that supercritical water can also be a good reaction medium for the hydrothermal synthesis of ZnO nanoparticles. Spherical ZnO nanoparticles were synthesized by oxidation of zinc acetate in supercritical water in a continuous tubular reactor. Particle size and morphology can be controlled by varying conditions like temperature, pressure or the reaction atmosphere. Nanoparticles with diameters ranging between 39 and 320 nm were synthesized using this method. The synthesis time has been significantly reduced through the use of microwave irradiation and the ZnO nanocrystallites thus formed were observed to be more defective than the ones synthesized over a few hours of hydrolysis. Nanoparticles with inherent defects are capable of exhibiting visible light photocatalysis even without doping with transition metals, which is the normally followed method. (Ali et al, 2016)

### 1.7.2 Milling Process

The mechanochemical process is a cheap and simple method of obtaining nanoparticles on large scale. (Baláz et al, 2013)

It involves high-energy dry milling, which initiates a reaction through ball–powder impacts in a ball mill, at low temperature. A thinner is added to the system in the form of a solid (usually NaCl), which acts as a reaction medium and separates the nanoparticles being formed. A fundamental difficulty in this method is the uniform grinding of the powder and reduction of grains to the required size, which decreases with increasing time and energy of milling. Unfortunately, a longer milling time leads to a greater quantity of impurities. The advantages of this method are the low production costs, small particle sizes and limited tendency for particles to agglomerate, as well as the high homogeneity of the crystalline structure and morphology. The starting materials used in the mechanochemical method are mainly anhydrous ZnCl<sub>2</sub> and Na<sub>2</sub>CO<sub>3</sub>. NaCl is added to the system; this serves as a reaction medium and separates the nanoparticles. The zinc oxide precursor formed, ZnCO<sub>3</sub>, is calcined at a temperature of 400–800 °C. The process as a whole involves the following reactions (1) and (2):



Temperature



The mechanochemical method was proposed by Ao et al. they synthesized ZnO with an average crystallite size of 21 nm. The milling process was carried out for 6 h, producing ZnCO<sub>3</sub> as the zinc oxide precursor. Calcination of the precursor at 600 °C produced ZnO with a hexagonal structure. Tests showed that the size of the ZnO crystallites depends on the milling time and calcination temperature. Increasing the milling time (2–6 h) led to a reduction in the crystallite sizes (21.5–25 nm), which may indicate the existence of a critical moment. Meanwhile an increase in the calcination temperature from 400 to 800 °C caused an increase in crystallite size (18–35 nm), the same system of reagents was used by. (Kołodziejczak et al, 2014)

They found that a milling time of 4 h was enough for a reaction to take place between the substrates, producing the precursor ZnCO<sub>3</sub>, which when calcined at 400 °C produced nanocrystallites of ZnO with an average size of 26 nm. Tsuzuki et al. showed that milling of the substrates without a thinner leads to the formation of aggregates measuring 100–1000 nm. This confirmed the important role played by sodium chloride in preventing agglomeration of the nanoparticles.

A milling process of ZnCl<sub>2</sub> and Na<sub>2</sub>CO<sub>3</sub> was also carried out by Moballegh et al and by Aghababazadeh et al. Moballegh et al., investigated the effect of calcination temperature on particle size. An increase in the temperature of the process (300–450 °C) caused an increase in the size of the ZnO particles (27–56 nm). Aghababazadeh et al. obtained ZnO with an average particle size of approximately 51 nm and a surface area of 23 m<sup>2</sup>/g, carrying out the process at a temperature of 400 °C. (Ali et al, 2016)

extended their previous study to investigate mechanical-thermal synthesis (MTS) mechanical activation followed by thermal activation of ZnO from ZnCl<sub>2</sub> and oxalic acid (C<sub>2</sub>H<sub>2</sub>O<sub>4</sub>·2H<sub>2</sub>O) as reactants with the intention of obtaining pure ZnO nanopowder. The study also aimed to examine the effects of oxalic acid as an organic, and different milling times, on the crystal structure, average particle size and morphology of ZnO nanopowders. The mixture of initial reactants was milled from 30 min up to 4 h, and subsequently annealed at 450 °C for 1 h. (Kołodziejczak et al, 2014)

Qualitative analysis of the prepared powders was performed using X-ray diffraction (XRD) and Raman spectroscopy. The XRD analysis showed perfect long-range order and the pure wurtzite structure of the synthesized ZnO powders, irrespective of the milling duration. By contrast, Raman spectroscopy indicates a different middle-range order of ZnO powders. From the SEM images, it is observed that the morphology of the particles strongly depends on the milling time of the reactant

mixture, regardless further thermal treatment. A longer time of milling led to a smaller particle size. (Kołodziejczak et al, 2014)

### **1.7.3 Chemical Bath Deposition**

The chemical bath deposition technique is, simple, environmental friendly, and yields well-oriented ZnO nanorods at growth temperatures down to  $\geq 90^{\circ}\text{C}$ , at the same time it is suitable for large area growth. The growth procedures involve precoating the substrate with ZnO nanoparticles followed by a postgrowth  $250^{\circ}\text{C}$  annealing step. The coating layer acts as a preferential growth site during the growth process and also improves the c-axis orientation of the grown ZnO nanorods. (Zainelabdin et al, 2010)

The precoated substrate is then immersed in an aqueous solution coatings Zn precursor material and a pH adjusting chemical agent. In a few reports, the growth of ZnO NRAs was performed at a lower temperature down to  $50^{\circ}\text{C}$ , but either a high temperature treatment ( $300^{\circ}\text{C}$ ) for the precoating layer or the ZNRAs were grown as free-standing, that is, without a substrate. The growth of well-aligned ZNRAs at  $50^{\circ}\text{C}$  without any other heat treatment is of interest for the growth on flexible plastic substrates, for example, organic p- polymers on flexible plastic for hybrid white light emitting diodes (LEDs) applications. In addition, some other p-type substrates are of interest to be integrated with ZNRAs to form p-n heterojunctions. This is due to the lack of stable reproducible p-type doping for ZnO material. Examples of an interesting p-type substrate are copper oxides ( $\text{CuO}$  and  $\text{Cu}_2\text{O}$ ) and organic semiconductors. Finally, metal layers are also of interest to be used as substrates for ZnO with the advantage of forming a contact at the bottom. Examples of interesting metals are silver (Ag) and copper (Cu). (Zainelabdin, et al, 2010)

### **1.8 Crystal structure of ZnO**

Crystalline ZnO has a wurtzite structure, a hexagonal unit cell with two lattice parameters,  $a$  and  $c$ , and belongs to the space group of  $C6v$  or  $P63mc$ . Figure 1 clearly shows that the structure is composed of two interpenetrating hexagonal closed packed (hcp) sublattices, in which each consist of one type of atom (Zn or O) displaced with respect to each other along the threefold c-axis. It Crystalline ZnO has a wurtzite (B4) crystal structure at ambient conditions. The ZnO can be simply explained schematically as a number of alternating planes stacked layer-by-layer along the c-axis direction and composed of tetrahedrally coordinated  $\text{Zn}^{2+}$  and  $\text{O}^{2-}$ . The tetrahedral coordination of ZnO gives rise to the noncentrosymmetric structure. In wurtzite hexagonal ZnO, each anion is surrounded by four cations at the corners of the tetrahedron, which shows the

tetrahedral coordination and hence exhibits the  $sp^3$  covalent-bonding.

Due to its vast areas of application, various synthetic methods have been employed to grow a variety of ZnO nanostructures, including nanoparticles, nanowires, nanorods, nanotubes, nanobelts, and other complex morphologies. (Gomez et al, 2013)

### 1.9 ZnO Nanoparticles Structure

The tetrahedral coordination of Zn-O is shown. O atoms are shown as larger white spheres while the Zn atoms are smaller brown spheres. Fig (1.1)

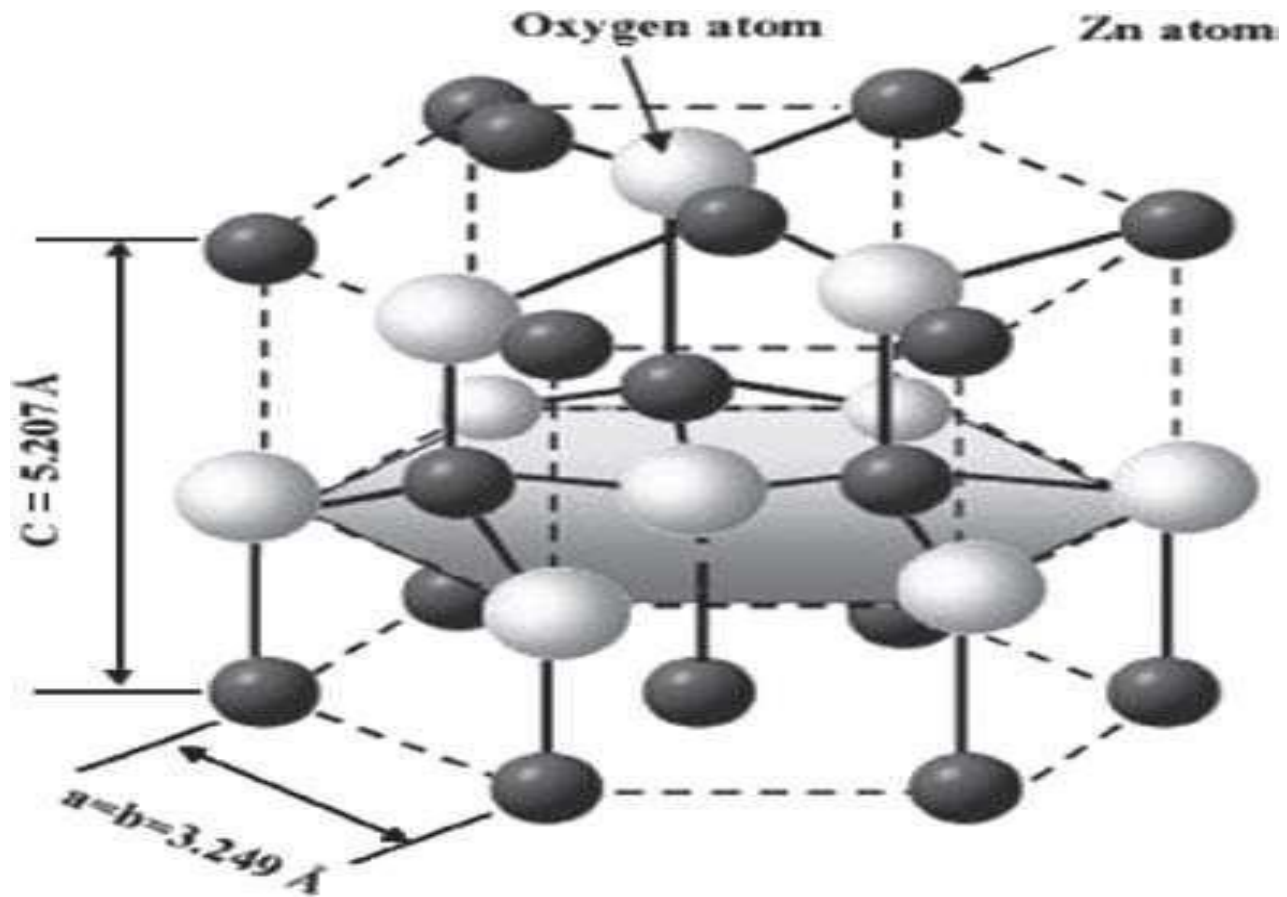


Figure (1.1): The Hexagonal Wurtzite Structure Model of ZnO.

Factors that affect the morphology of ZnO nanoparticles: are

1-Reaction condition

2- Solvent.

3-pH

4-Water addition.

5-Reactant concentration.

Synthesis of ZnO nanoparticles solution requires a well-defined shape and size of ZnO nanoparticles. In this regards, reported room- temperature organometallic synthesis of ZnO nanoparticles of controlled shape and size in solution.( Vaseem et al,2010)

The principle of this experiment was based on the decomposition of organometallic precursor to the oxidized material in air. It was reported that when a solution of dicyclohexylzinc(II) compound  $[Zn(c-C_6H_{11})_2]$  in tetrahydrofuran (THF) was left standing at room temperature in open air, the solvent evaporated slowly and left a white luminescent residue, which was further characterized by X-ray diffraction (XRD) and transmission electron microscopy (TEM) and as agglomerated ZnO nanoparticles with a zincite structure having lack of defined shape and size.confirmed. used a modified experimental condition using a ligand of long chain amine, i.e., hexadecylamine (HDA) under an argon atmosphere in addition to the above- mentioned solution, which resulted in well- defined ZnO nanoparticles. It was observed that shape, size, and homogeneity of the as- synthesized products depend upon various reactions conditions, i.e., the nature of the ligand, the relative concentration of reagents, the solvent, the overall concentration of reagents, the reaction time, the evaporation time, and the reaction/evaporation temperature. In addition, when a similar reaction . is carried out in dry air, it leads to agglomerated ZnO nanoparticles displaying no defined shape or size. In an elaborative manner, they analyzed that if the concentration of reagents in solution increases from 0.042 to 0.125 mol L<sup>-1</sup> nano-objects of higher aspect ratio will be formed. Exchanging THF for toluene or heptane produces nanoparticles of isotropic morphology with mean diameters of 4.6 for toluene and 2.4 nm for heptane.

A slow oxidation tow weeks evaporation process in THF produces only very homogenous nanodisks having size 4.1 nm (Fig1.2). Reducing the reaction time under argon to 5 min prior to oxidation leads to shorter nanorods  $\sim 5.8 \times 2.7$  nm in size. Increasing the reaction temperature

leads to isotropic disk-shaped nanoparticles. Exchanging HDA for dodecylamine (DDA) or octylamine (OA) also leads to disks with mean diameters of 3.0 for DDA and 4.0 nm for OA (Figs.1.2(c and d)). In addition, nuclear magnetic resonance (NMR) studies confirmed that throughout the oxidation process, the amine ligand remains coordinated to zinc and suggested that this coordination participates in controlling the growth of ZnO nanoparticles. Vaseem et al,2010) reported the detailed experimental procedure based on the same synthetic route with different experimental parameters, i.e., the effects of solvent, ligand, concentration, time, and temperature. They explained that the reaction of organometallic complexes with oxygen or moisture leads exothermally to a hydroxide material, but in this case they did not observe any traces of hydroxide

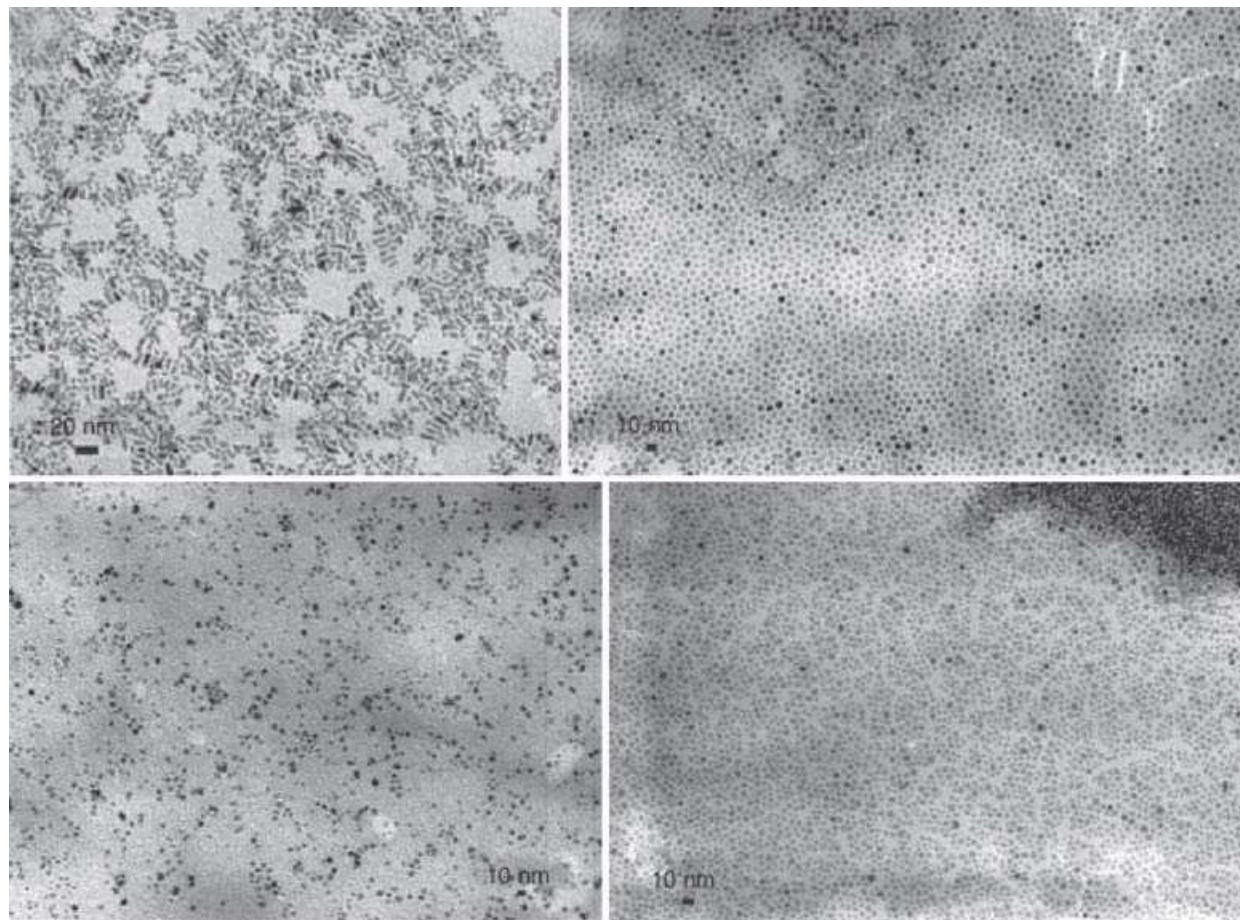


**Figure (1.2): TEM Micrographs of ZnO Nanoparticles.**

- (a) ZnO nanorods grown under standard conditions.
- (b) ZnO nanodisks following a slow, two weeks oxidation/evaporation process in THF
- (c) ZnO nanodisks using DDA instead of HDA as the stabilizing ligand under standard conditions.
- (d) ZnO nanodisks using OA instead of HDA under standard conditions. The solvent has an important effect on the morphology of ZnO nano-objec.

To show the effect of acidic and basic solution routes on the morphology of ZnO, Vaseem et al, (2010) synthesized ZnO nanoparticles with various aspect ratios. In a typical synthetic process, ZnO grains and ZnO rods were obtained with various aspect ratios at 60°C with 2 h reaction in aqueous solution of ZnSO<sub>4</sub> via an acidic route (pH 5.6) with addition of NaOH and in a basic solution of NaOH (pH 13.6) with addition of ZnSO<sub>4</sub>, respectively. The observed aspect ratios changed, although the final pH of the solution was the same. The detailed morphological characterizations were performed by XRD, field emission scanning electron microscopy (FESEM), and field emission transmission electron microscopy (FETEM). XRD analysis confirmed the wurtzite ZnO type structures with peak broadening in the case of the acidic pH compared to the alkaline pH, which further confirmed the formation of smaller particles via the acidic route. FESEM images also confirmed the formation of ZnO particles and rods via acidic and basic routes, respectively. Further cumulative undersize distribution of precipitated ZnO particles confirmed that the particle shapes were spherical or ellipsoidal with diameters of 32 and 44 nm, respectively, via the acidic route at pH 12.8, which were consistent with the crystallite size calculated by Scherrer's formula using the (100) and (002) diffraction peaks observed in XRD spectra. Although the value of  $[\text{OH}^-]/[\text{Zn}^{2+}]$  and the final pH were the same in the acidic and basic routes, the number of ZnO nuclei formed via the acidic pH was deduced to be much higher than that obtained via the basic pH because the degree of saturation at the initial stage of the acidic route was extremely high due to the low solubility of ZnO. Thus, most of the precursor species steeply precipitated as nanograins. On the other hand, ZnO nanorods formed in the basic route due to limitation of formed ZnO nuclei at the initial stage, and thus particle size increased via subsequent growth in the progressive stage. To check the effect of water addition in the precursor-methanol solution for the morphological Evolution of ZnO particles, Waseem et al, (2010) performed reactions based on hydrolysis of zinc acetate in methanol solvent at 60°C for 24 h and deposited over Al<sub>2</sub>O<sub>3</sub> ceramic plate via the chemical deposition method. As the water/methanol volume ratio increased, the shape of the ZnO particles changed from irregular

particles to plates and then from plates to regular cones, including the size change from nanoscale to micro-scale. In addition, if the volume of added water increased, the height of the cones decreased. Addition of water controlled the hydrolysis of zinc acetate and affected the nucleation process of ZnO significantly. Moreover, addition of water can impede the [0001] growth and accelerate the [11 00] growth if the volume ratio of added water/methanol is equal to or greater than 2:15. In this way, the shape and size of ZnO can be tailored by adjusting the volume ratio.

During the synthesis of ZnO nanoparticles, the influences of the reactant concentration were reported by. (Zhang et al,2019)

In a typical process, ZnO nanoparticles were synthesized by using zinc acetate and NaOH in 2-propanol solution. As the nucleation and growth were fast in this synthetic process, at longer times the particle size was controlled by coarsening. In addition, coarsening kinetics were independent of the zinc acetate concentration from 0.5–1.25 mM at a fixed [zinc acetate: NaOH] ratio of 0.625. The width of the size distribution increased slightly time. Moreover, if the zinc acetate concentration was fixed at 1 mM, the kinetics were independent of variation in the [zinc acetate: NaOH] ratio from 0.476–0.625. The presence of water in the reaction mixture was checked, and it was found that at low water concentration, the nucleation and growth of ZnO were very slow, which only slightly affected the coarsening kinetics for water content above ~20 mM Thus, by this synthesis method, it is confirmed that

ZnO nanoparticles are insensitive to the reactant concentration and presence of water.

The control of the shape and the orientation of nano-/ micro crystallites as well as the ability to order them into large three-dimensional arrays onto various types of substrates represent essential tasks to fulfill in order to create a future generation of smart and functional materials. Hitherto, the competence to generate aligned and ordered crystallites onto substrates was essentially based on template/membrane synthesis, patterning techniques, or epitaxial electrode position.

The strategy to control the shape and orientation of crystallites consists of growing thin- film materials directly onto substrates, from the molecular scale to the nano-/mesoscale, from aqueous precursors in solution by monitoring the thermodynamics and kinetics of nucleation and growth of the materials by experimentally controlling its interfacial tension. This approach led to the development of a novel general concept, namely, purpose built materials which is dedicated to the design of novel metal oxide materials with the appropriate morphology, texture, and orientation in order to probe, tune, and optimize their physical properties.( Vayssieres et al,2001)

In most cases, homogeneous nucleation of solid phases (metal oxides in particular) requires a higher activation energy barrier, and therefore, heteronucleation will be promoted and will be energetically more favorable (e.g., influence of seeding on crystal growth). Indeed, the interfacial energy between crystals and substrates is usually smaller than the interfacial energy between crystals and solutions. Consequently, (hetero) nucleation takes place at a lower saturation ratio onto a substrate than in homogeneous solution. Epitaxial crystal growth occurs from substrate-generated nuclei along the easy direction of crystallization, and if the concentration of precursors is high, a condensed phase, of single-crystalline rods perpendicular to the substrate, is obtained. Recently, such approach has been successfully applied to the design of large arrays of three dimensional crystalline highly oriented hematite nanorod array, whose unique structural design led to a two-dimensional quantum confinement as well as an incident photon-to-electron conversion efficiency (IPCE) of 60% at 350nm. (Vayssieres et al, 2001)

## 1.10 Characterization of Zinc Oxide Nanoparticles

### 1.10.1 X-ray Diffraction Analysis

XRD diffraction pattern of ZnO nanoparticles figure 1.3 .The peaks are indexed as  $31.82^\circ$  (100),  $34.54^\circ$  (002),  $36.42^\circ$  (101),  $47.46^\circ$  (102),  $56.74^\circ$  (110),  $62.92^\circ$  (103),  $66.06^\circ$  (200),  $68.42^\circ$  (112),  $69.06^\circ$  (201) and  $78.82^\circ$  (202) respectively. All diffraction peaks of sample correspond to the characteristic hexagonal wurtzite structure of zinc oxide nanoparticles ( $a = 0.315$  nm and  $c = 0.529$  nm). Similar, X-ray diffraction pattern were reported by (Roberson et. al, 2014), average particle size of ZnO nanoparticles is found to be 10.0 nm using Scherer equation. Diffraction pattern corresponding to impurities are found to be absent. This proves that pure ZnO nanoparticles were as synthesized.

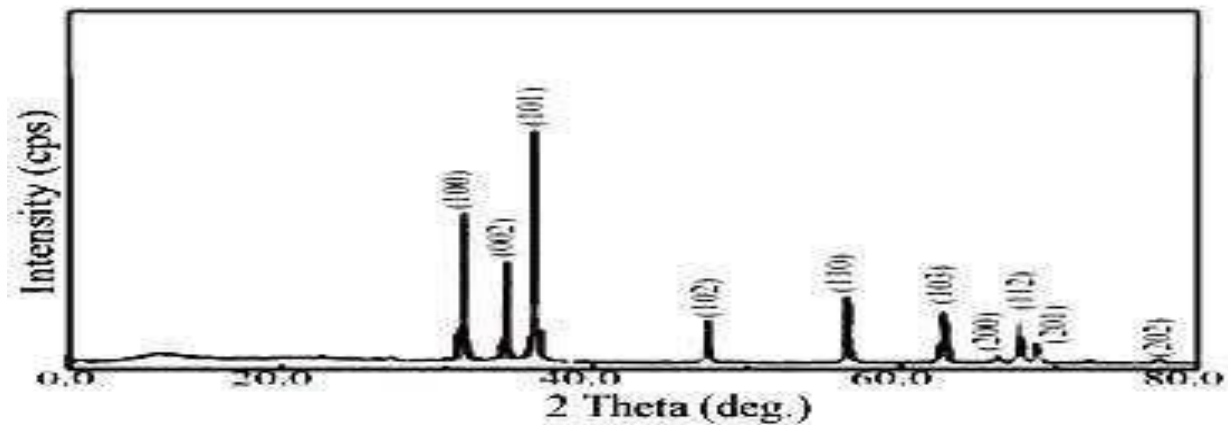
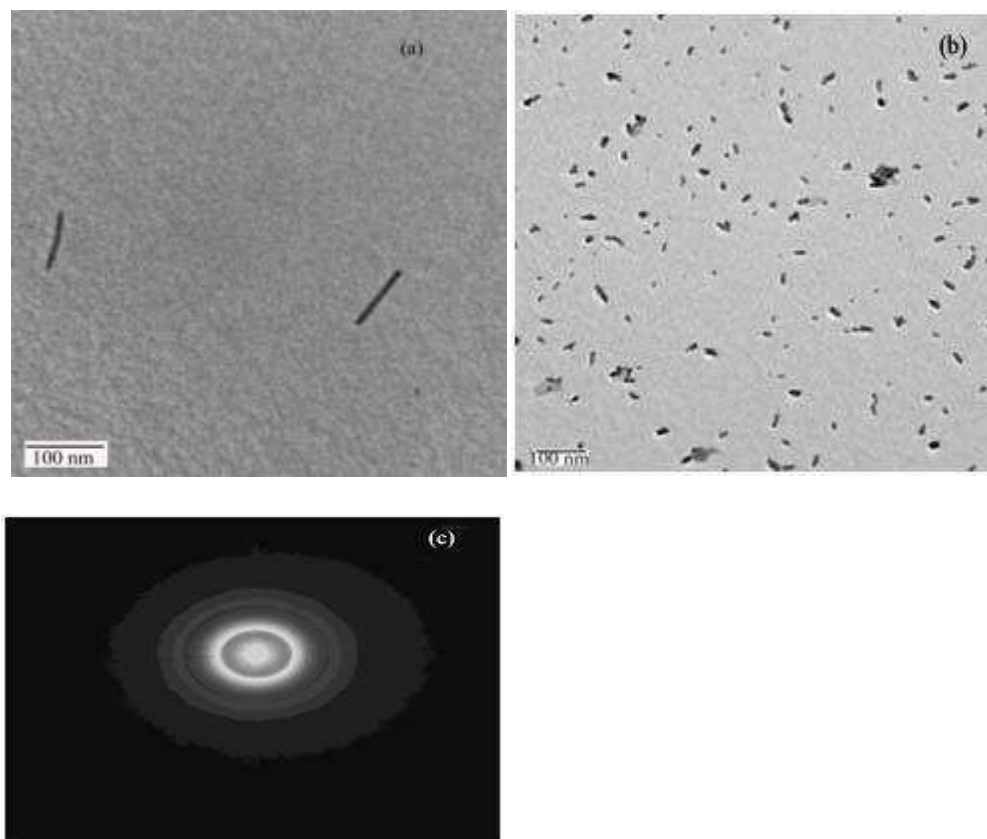


Figure (1.3): XRD Patterns of ZnO Nanoparticles

### 1.10.2 Transmission Electron Microscopy

TEM images of ZnO nanoparticles were shown in Figure (1.4). Rod shape ZnO nanoparticles were observed in TEM images of average size in the range of 10.0-12.0 nm which is in good agreement with the size calculated by XRD. Figure(1.4) (c) shows the selected area diffraction pattern (SAED) of ZnO nanoparticles. It shows that the particles are well crystallized. The diffraction rings on SAED image matches with the peaks in XRD pattern which also proves the hexagonal wurtzite structure of ZnO nanoparticles. Rod shape ZnO nanoparticles were observed in TEM images of average size in the range of 10.0-12.0 nm which is in the good agreement with the size calculated by XRD. Figure4 (c) shows the selected area diffraction pattern (SAED) of ZnO nanoparticles. It shows that the particles are well crystallized. The

Diffraction rings on SAED image matches with the peaks in XRD pattern which also proves the hexagonal wurtzite structure



**Figure (1.4): TEM Images of ZnO Nanoparticles (a, b) and its Selected area Electron Diffraction Image (c).**

### 1.10.3 FTIR spectroscopy

FTIR spectrum of ZnO nanoparticles was shown in Figure (1.5). Infrared studies were carried out in order to ascertain the purity and nature of the metal nanoparticles. Metal oxides generally give absorption bands in fingerprint region i.e. below  $1000\text{ cm}^{-1}$  arising from inter-atomic vibrations. The peak observed at  $3452.30$  and  $1119.15\text{ cm}^{-1}$  are may be due to O-H stretching and deformation, respectively assigned to the water adsorption on the metal surface. The peaks at  $1634.00$ ,  $620.93\text{ cm}^{-1}$  are corresponding to Zn-O stretching and deformation vibration, respectively. The metal-oxygen frequencies observed for the respective metal oxides (Mahamuni et al,2019) reported similar FTIR spectra observed of zinc oxide nanoparticles in their investigation.

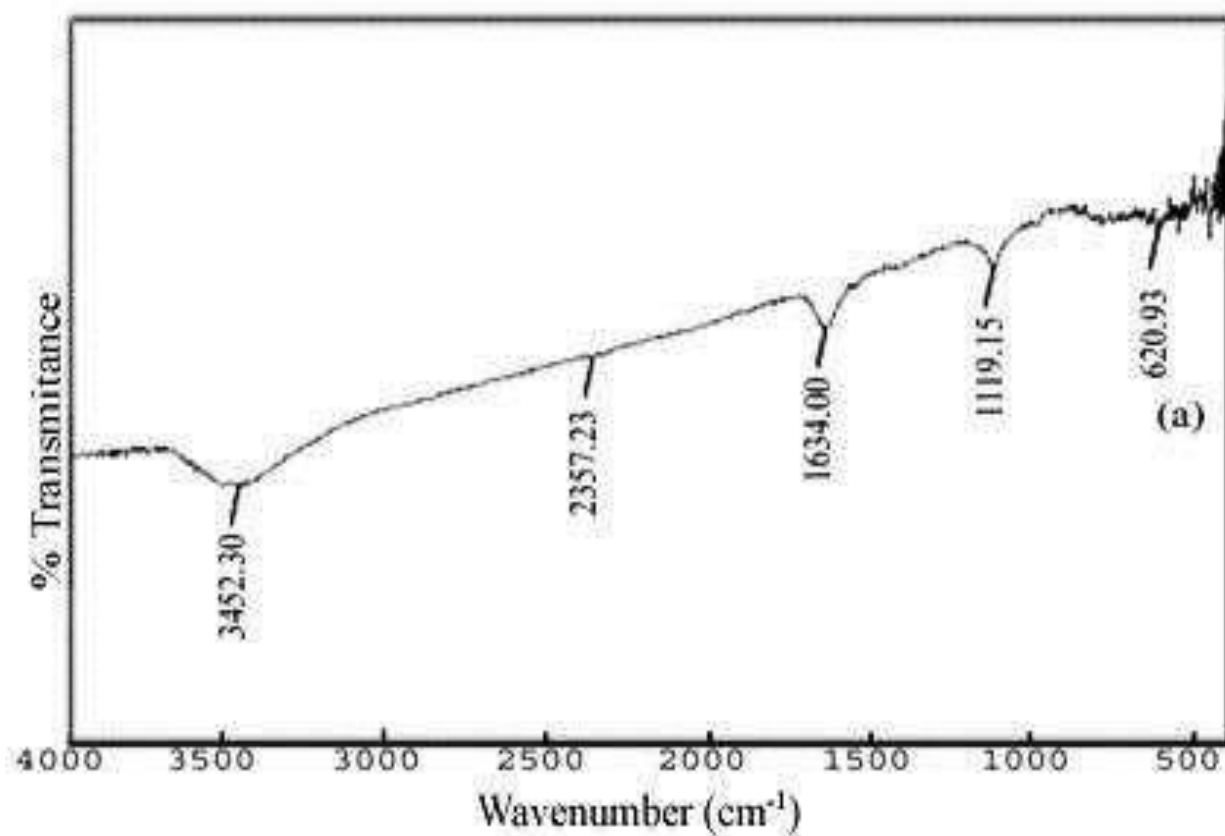


Figure (1.5): FTIR Spectra of ZnO Nanoparticles

### 1.10.4 UV-Visible spectroscopy

The optical characterization of the sample was recorded on UV-Vis absorption spectrophotometer. Figure (1- 6) (a) shows the UV-Visible absorption spectra of ZnO nanoparticles as a function of wavelength. The UV-Visible absorption spectroscopy of ZnO nanoparticles in ethanol shows an excitonic absorption peak at about 214 nm, which lies much below the band gap wavelength of 388 nm of bulk ZnO. The peak at 214 nm is due to interband transition of copper electron from deep level of valence band. The blue shift in the peak centered at 214 nm in absorption spectra (Figure 1. 6, a) may be due to the transition of electrons from the more inner to the uppermost shell as time passes. It is possible that, due to aggregation and agglomeration, particle size increases and material settled down on the bottom of container causing decrease in the absorbance. This behavior is typical for many semiconductors due to internal electric fields within the crystal and inelastic scattering of charge carriers by phonons. Absorption coefficient ( $\alpha$ ) associated with the strong absorption region of the sample was calculated from absorbent (A) and the sample thickness (t) was used the relation. (Kumar et al,2013)

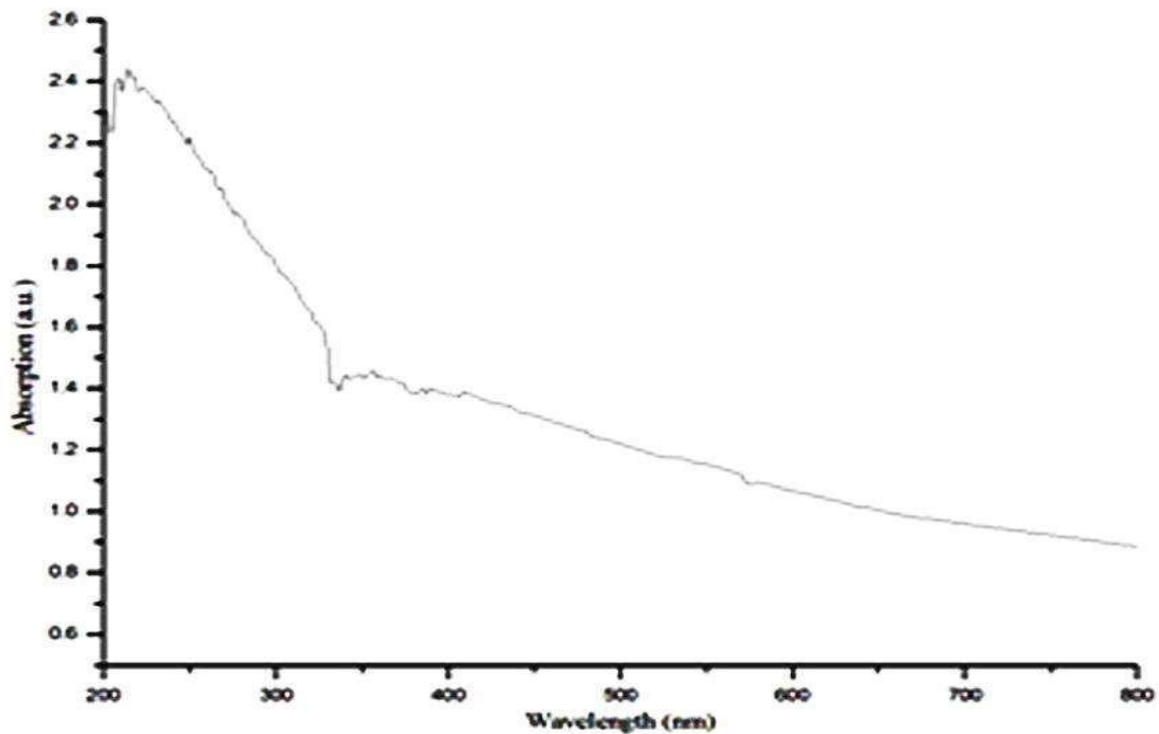
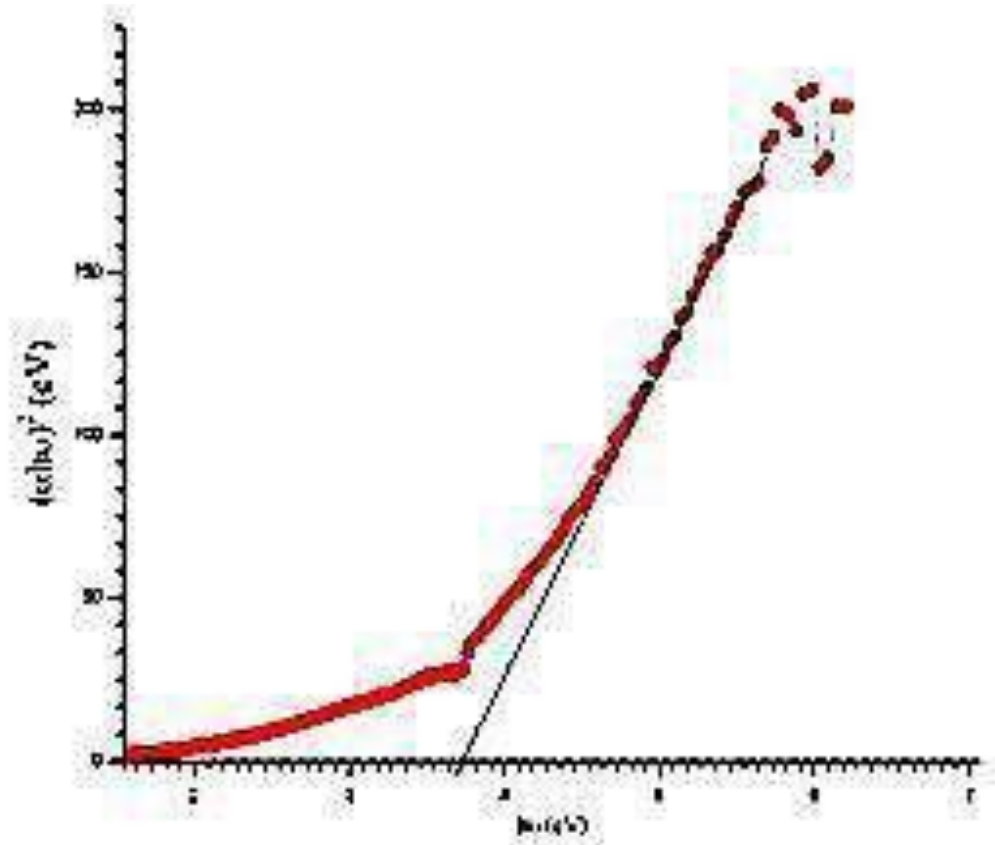


Figure (1. 6) (a): Absorption of ZnO Nanoparticles as a Function of Wavelength



**Figure (1.6) (b):Variation of  $(\alpha h\nu)^2$  with  $h\nu$  for ZnO Nanoparticles as a Function of Wavelength at  $1/2$  n Value**

$$\alpha = 2.303A/t \quad (3)$$

While the optical band gap of ZnO nanoparticles is calculated using the Tauc relation

$$\alpha = B (h\nu - E_g)^n / h\nu \quad (4) \text{ (Moloantoa et al,2016)}$$

Where,  $\alpha$  is the absorption coefficient, B is a constant,  $h\nu$  is the energy of incident photons and exponents n whose value depends upon the type the transition which may have values  $1/2$ , 2,  $3/2$  and 3 corresponding to the allowed direct, allowed indirect, forbidden direct and forbidden indirect transitions, respectively. Figure (1.6) (b) show the variation of  $(\alpha h\nu)^{1/n}$  vs. photon energy,  $h\nu$  for ZnO nanoparticles with n values of  $1/2$ . Allowed direct band gap of ZnO nanoparticles is calculated to be 3.7 eV, which is higher than reported value 3.5348 eV. The increase in the band gap of the ZnO nanoparticles with the decrease in particle size may be due to a quantum confinement effect. (S.K., et al (2009))

### 1.10.5. DSC analysis

The isothermal oxidation behavior and the oxidized structure of ZnO nanoparticles have been investigated using DSC technique over a temperature range of 50-600 °C in ambient air. Figure (1.7) shows DSC curve of zinc oxide nanoparticles. A small low temperature endothermic peak at 138.81 °C is due to loss of volatile surfactant molecule adsorbed on the surface of zinc oxide nanoparticles during synthesis conditions. A large high temperature endothermic peak at 260.43°C is assigned the conversion of zinc hydroxide to zinc oxide nanoparticles. A small high temperature endothermic peak at 382.77 °C attributed the conversion of zinc oxide into zinc nanoparticles. (Kumar et al., 2013)

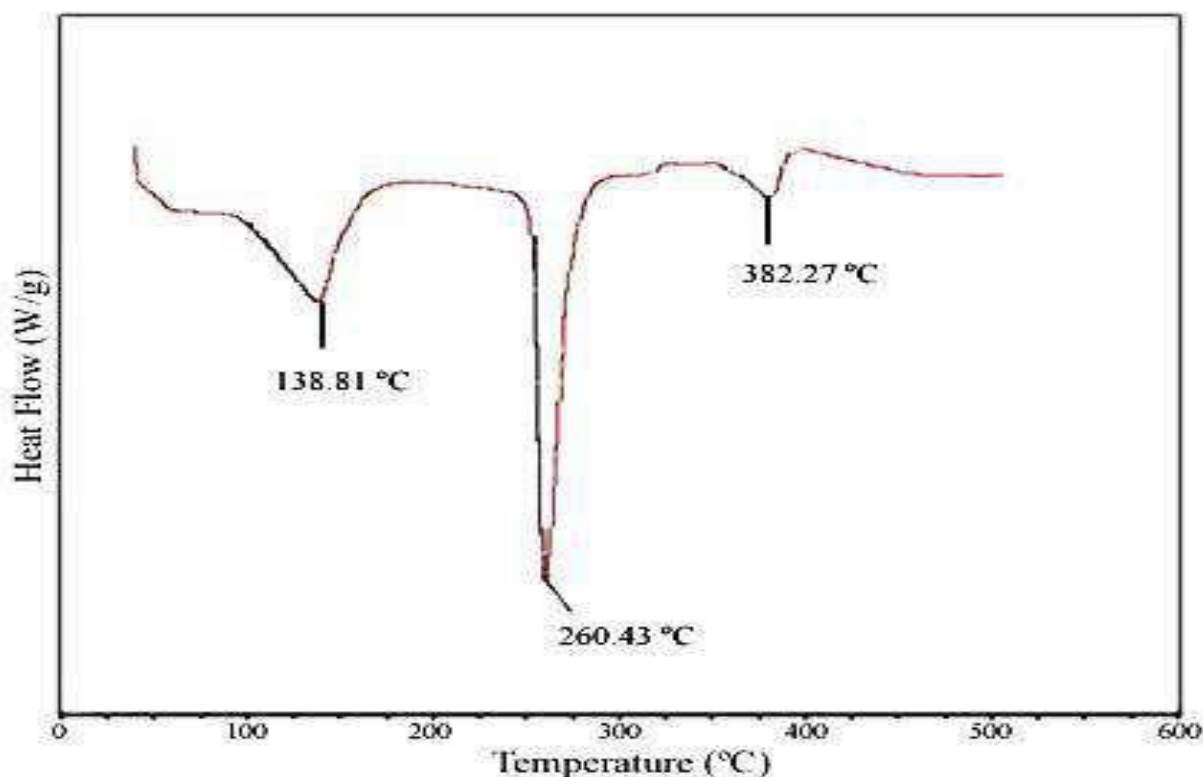


Figure (1.7): DSC Curve of ZnO Nanoparticles

### Applications of ZnO nanostructures

Because of its diverse chemical and physical properties zinc oxide plays an important role in a very wide range of applications, ranging from tyres to ceramics, from pharmaceuticals to agriculture, and from paints to chemicals. Figure 1.9 summarized application paths of ZnO.

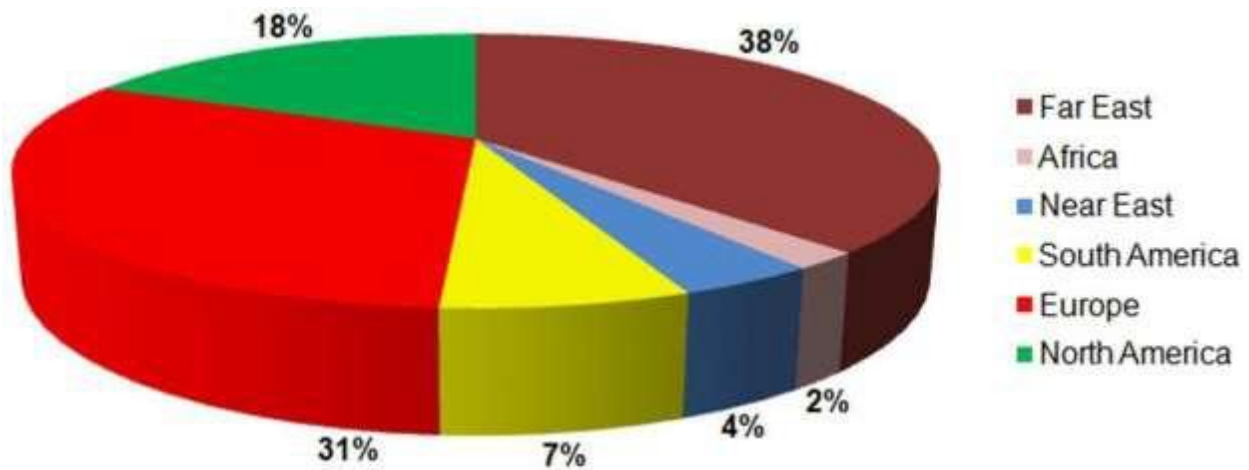


Figure (1.8): Worldwide Consumption of Zinc Oxide.

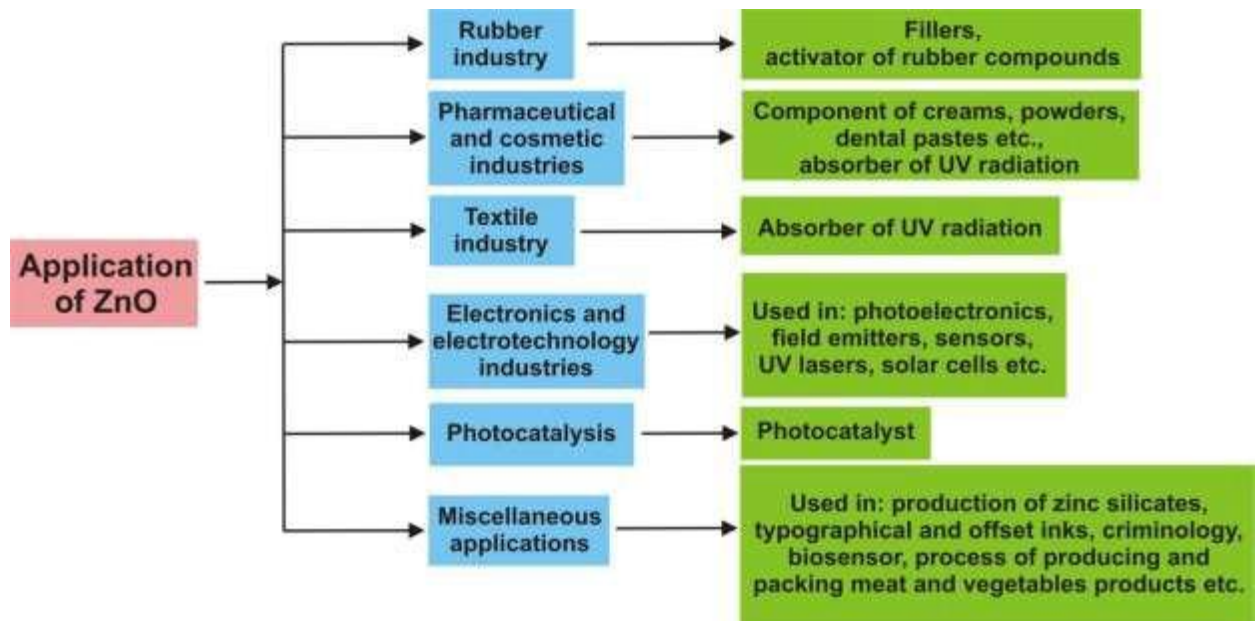


Figure (1.9): Schematic Representation the Application of ZnO.

### 1.11 Literature review

A large fraction of the ZnO, currently produced, is used in the rubber and concrete industries ZnO is an important additive to the rubber of car tyres. It has a positive influence on the vulcanisation process, and it considerably improves the heat conductivity, which is crucial to dissipate the heat produced by the deformation when the tyre rolls along the street. In concrete, an admixture of

ZnO allows an increase in the processing time and improves the resistance of concrete against water. Other applications concern medicine or cosmetics. ZnO is used as an UV-blocker in suntan lotions or as an additive to human and Animals food. Furthermore, it is used as one component of mixed-oxide varistors, devices which allow voltage limiting.

Due to its wide band gap, ZnO is transparent in the visible part of the electromagnetic Spectrum. Highly n-doped ZnO: Al can therefore be used as a transparent conducting oxide (TCO). The constituents Zn and Al are much cheaper and less poisonous compared to the generally used indium tin oxide (ITO). One application which has begun to be commercially available is the use of ZnO as the front contact for solar cells, which avoids the shadow effect necessarily associated with metal- finger contacts. Other appearing applications use ZnO as the front contact of liquid crystal displays or ZnO : Al in the production of energy-saving or heat-protecting windows. A coating with TCO results in a glass which lets the visible part of the spectrum in but either reflects the IR back into the room (energy saving) or does not let the IR radiation into the room (heat protection), depending on which side of the window has the TCO coating. (lingshirn et al, 2007)

Using zinc oxide (ZnO) nanostructures, nanorods (NRs) and nanoparticles (NPs) grown on different substrates (submicrometer glass pipettes, thin silver wire and on plastic substrate) different bio-sensors were demonstrated. The demonstrated sensors are based on potentiometric approach and are sensitive to the ionic metals and biological analyte in question. For each case a selective membrane or enzyme was used. The measurements were performed for intracellular environment as well as in some cases (cholesterol and uric acid). The selectivity in each case is tuned according to the element to be sensed. Moreover we also developed photodynamic therapy approach based on the use of ZnO NRs and NPs. Necrosis/apoptosis was possible to achieve for different types of cancerous cell. The results indicate that the ZnO with its UV and white band emissions is beneficial to photodynamic therapy technology.

ZnO possesses high Isoelectric Point (IEP) of 9.5 which makes it suitable for absorption of proteins with low IEPs where the protein immobilization is primarily driven by electrostatic interaction. (Willander et al, 2011)

ZnO The fabrication and application of an intracellular  $K^+$  -selective microelectrode is demonstrated. ZnO nanowires with diameter of 100–180nm and a length of approximately 1.5 $\mu$ m are grown on a borosilicate glass microcapillary. ZnO nanowires coated by a  $K^+$  -

ionophore-containing membrane. The  $K^+$  selective microelectrode exhibited a  $K^+$  - dependent potentiometric response versus an Ag/AgCl reference microelectrode that was linear over a large concentration range (25  $\mu$ M–125 mM) with a minimum detection limit of 1  $\mu$ M. The measured  $K^+$  concentrations in human adipocytes and in frog oocytes were consistent with values of  $K^+$  concentrations reported in the literature (Ali, et al, 2011). The sensor has several advantages including ease of fabrication, ease of insertion into the cells, low cost, and high selectivity features that make this type of sensor suitable to characterize physiologically relevant ions within single living cells.

An electrochemical biosensor based on ZnO nanorods for potentiometric cholesterol determination is proposed. Hexagon-shaped ZnO nanorods were directly grown on a silver wire having a diameter of 250  $\mu$  m using low temperature aqueous chemical approach that produced ZnO nanorods with a diameter of 125– 250 nm and a length of  $\sim$ 1  $\mu$ m. Cholesterol oxidase (ChOx) was immobilized by a physical adsorption method onto ZnO nanorods. The electrochemical response of the ChOx/ZnO/Ag biosensor against a standard reference electrode (Ag/AgCl) was investigated as a logarithmic function of the cholesterol concentration ( $1 \times 10^{-6}$  M to  $1 \times 10^{-2}$  M) showing good linearity with a sensitivity of 35.2 mV per decade and the stable output signal was attained at around 10 s. (Israr et al, 2010)

ZnO nanorods (NRs) with high surface area to volume ratio and biocompatibility is used as an efficient photosensitizer carrier system and at the same time providing intrinsic white light needed to achieve cancer cell necrosis. In this letter, ZnO nanorods used for the treatment of breast cancer cell (T47D) are presented. To adjust the sample for intracellular experiments, we have grown the ZnO nanorods on the tip of borosilicate glass capillaries (0.5 mm diameter) by aqueous chemical growth technique. The grown ZnO nanorods were conjugated using protoporphyrin dimethyl ester (PPDME), which absorbs the light emitted by the ZnO nanorods. Mechanism of cytotoxicity appears to involve the generation of singlet oxygen inside the cell. The novel findings of cell- localized toxicity indicate a potential application of PPDME-conjugated ZnO NRs in the necrosis of breast cancer cell within few minutes. (Kishwari et al, 2010)

ZnO nanorods were grown on a silver-coated tip of a borosilicate glass capillary (0.7 mm tip diameter) and used as selective potentiometric sensor of intracellular free  $Mg^{2+}$ . To functionalize the ZnO nanorods for selectivity of  $Mg^{2+}$ , a polymeric membrane with  $Mg^{2+}$ -selective ionophores were coated on the surface of the ZnO nanorods. These functionalized ZnO

nanorods exhibited a  $Mg^{2+}$ -dependent electrochemical potential difference versus an Ag/AgCl reference microelectrode within the concentration range from 500 nM to 100 mM. Two types of cells, human adipocytes and frog oocytes, were used for the intracellular  $Mg^{2+}$  measurements. The intracellular concentration of free  $Mg^{2+}$  in human adipocytes and frog oocytes were 0.4–0.5 and 0.8–0.9 mM, respectively. Such type of nanoelectrode device paves the way to enable analytical measurements in single living cells and to sense other bio-chemical species at the intracellular level. (Asif et al, 2010)

Demonstrate hydrothermal synthesis of coral-like CuO nanostructures by selective growth on ZnO nanorods (NRs) at low temperatures. During the hydrothermal processing the resulting hydroxylated and eroded surface of ZnO NRs becomes favorable for the CuO nanostructures growth via oriented attachments. Heterojunction p–n diodes fabricated from the CuO/ZnO nanocorals (NCs) reveal stable and high rectification diode properties with a turn-on voltage of  $\sim 1.52$  V and a negligible reverse current. The humidity sensing characteristics of the CuO/ZnO NC diodes exhibit a remarkable linear (in a semilogarithmic scale) decrease in the DC resistance by more than three orders when the relative humidity changed from 30–90%. The NC humidity sensor is also found to reveal the highest sensitivity factor of  $\sim 6045$  among available data for the constituent materials and a response and recovery time of 6 s and 7 s, respectively. (Zainelabdin et al, 2012)

The inactivation of model microbes in aqueous matrix by visible light photocatalysis as mediated by ZnO nanorods was investigated (Bora et al 2017)

ZnO nanorods were grown on glass substrate following a hydrothermal route and employed in the inactivation of gram-negative *Escherichia coli* and gram-positive *Bacillus subtilis* in MilliQ water.

The concentration of  $Zn^{2+}$  ions in the aqueous matrix, bacterial cell membrane damage, and DNA degradation at post-exposure were also studied. (Pattison et al, 2012)

The inactivation efficiencies for both organisms under light conditions were about two times higher than under dark conditions across the cell concentrations assayed. Anomalies in supernatant  $Zn^{2+}$  concentration were observed under both conditions as compared to control treatments, while cell membrane damage and DNA degradation were observed only under light conditions. Inactivation under dark conditions was hence attributed to the bactericidal effect of  $Zn^{2+}$  ions, while inactivation under light conditions was due to the combined effects of  $Zn^{2+}$  ions

and photocatalytically mediated electron injection. The reduction of pathogenic bacterial densities by photocatalysis

Active ZnO nanorods in the presence of visible light meets potential application in water decontamination at ambient conditions under sunlight. (Sapkota et al, 2011)

We demonstrate intrinsic white light emission from hybrid light emitting diodes fabricated using an inorganic–organic hybrid junction grown at 50 °C on a paper substrate. Cyclotene was first spin coated on the entire substrate to act as a surface barrier layer for water and other nutrient solutions. The active area of the fabricated light emitting diode (LED) consists of zinc oxide nanorods (ZnO NRs) and a poly (9, 9-dioctylfluorene) (PFO) conducting polymer layer. The fabricated LED shows clear rectifying behavior and a broad band electroluminescence (EL) peak covering the whole visible spectrum range from 420 nm to 780 nm. The color rendering index (CRI) was calculated to be 94 and the correlated color temperature (CCT) of the LED was 3660K. The low process temperature and procedure in this work enables the use of paper substrate for the fabrication of low cost ZnO–polymer white LEDs for applications requiring flexible/disposable electronic device.( Amin et al,2012)

## **1.12 Objectives of The Study**

- 1- To prepare ZnO nanoparticles at high temperature
- 2- To prepare 5% Ni doped ZnO nanoparticles at high temperature
- 3- To characterize both ZnO and 5% Ni doped ZnO
- 4- To degrade of methyl orange by using both ZnO and 5% Ni doped ZnO
- 5- Kinetic study of degradation process

## Chapter Two

### Material and Methods

#### 2.1 Materials

##### 2.1.1 Chemicals

1- Nickel nitrate hexahydrate ( $\text{NiNO}_3\cdot 6\text{H}_2\text{O}$ )

a) Molecular weight 290.791g/mole

b) Density 2.05g/cm<sup>3</sup>

c) Melting point 134.1F (56.7C)

2- Zinc nitrate hexahydrate ( $\text{ZnNO}_3\cdot 6\text{H}_2\text{O}$ ) laboratory grade (LR)

Specification:

a) Molecular weight 297.49g/mole

b) Minimum assay 98.0% (complex metric)

c) PH of 10% solution in water

d) Chloride 0.005%

e) Sulphate ( $\text{SO}_4$ ) 0.01%

f) Iron (Fe) 0.005%

3- Sodium hydroxide pellets laboratory grade (LR)

Specification:

a) Assay (acidimetric) % min 97%

b) Carbonate (as  $\text{NaCO}_3$ )% max 1.0

c) Chloride (Cl) % max 0.01

d) Sulphate ( $\text{SO}_4$ )% max 0.002

e) Phosphate ( $\text{PO}_4$ )% max 0.002 deionized water

4- Methyl orange (module) batch NO TP040139 (toxic)

This substance is very hazardous to health when inhaled, swallowed or in contact with skin and may even lead to death.

a) Molecular weight 327.33

b) Chemical formula  $\text{C}_{14}\text{H}_{14}\text{N}_3\text{NaO}_3\text{S}$

## 2.2 Apparatus

- a) Beakers
- b) Measuring cylinder
- c) Glass rods
- d) Magnetic steerer
- e) Aluminum foil
- f) Ash less paper
- g) Conical flasks

## 2.3 Instruments

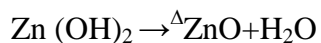
- a) Fourier Transform Infrared Spectrophotometer FTIR-8400S
- b) Drying Oven (CARBOLITE) England-moduel PF200-serial number 11/02/3073
- c) Magnetic stirring (heat-stir) CB162
- d) pH-meter pH/ORP/ISE meter (HANNA) Romania serial number (006024)
- e) Furnace (Nabertherm-germany) more than heat ((30—3000C<sub>o</sub> )) serial number 198236
- f) UV-VIS for characterization (Perkin Elmer LS55 luminescence)
  - a) UV-VIS for degradation (spectrophotometer (Labomed – UVS-2800))
  - b) Scanning electronic microscopic

## 2.4 Method

### 2.4.1 Synthesis of ZnO

The synthesis of ZnO is based on the reaction between Zinc nitrate hex hydrate and sodium hydroxide follow by calcinate of hydroxide

General equation



Procedure:-

30g of  $\text{Zn}(\text{NO}_3)_2 \cdot 6\text{H}_2\text{O}$  were dissolved in 300 ml of deionized water under vigorous stirring for 30 min, 8g of sodium hydroxide were dissolved in 100 ml deionized water with stirring, all volume of sodium hydroxide is added to the zinc nitrate hex hydrate solution under vigorous stirring. After adding all volume, excess of sodium hydroxide was added. The pH was maintained 12. (Lanje et al, 2013)

Mixture was left to stand for 12 hour , in covered container . top layer was, carefully, decanted and the precipitate was washed for times with deionized water and then with ethanol , filter and the filtrate was dried at 105° for one hour and finally calcinated at 700C .collected the precipitate for further characterization.

#### **2.4.2 Synthesis of 5% Ni doped ZnO**

28.5g of Zn (NO<sub>3</sub>)<sub>2</sub>.6H<sub>2</sub>O and 1.5g of Ni (NO<sub>3</sub>)<sub>2</sub>.6H<sub>2</sub>O ware dissolved in 300ml of deionized water by vigorous stirring using magnetic stirrer .To this solution 100 ml of aqueous solution of 8g sodium hydroxide was added drop wise, The pH was maintained 12.After the addition is completed the mixture was left to stand for 12 hour, top layer was, carefully, decanted and the precipitate was washed for times with deionized water and then with ethanol, filter and the filtrate was dried at 105° for one hour and finally calcinated at 700C .Collected the precipitate for further characterization.

#### **2.4.3 Scanning Electron Microscope Measurement**

Figure (2.1), used for morphology analysis. The SEM generates images by scanning the specimens using a focused electron beam. The electrons interact with atoms in the sample and produce different signals, used as surface information of the samples. The morphology of the nanopowder samples was examined, the samples were previously oven dried at 105C° for tow a hours and coated with a thin film of gold to provide ZnO powder surface with electrical conduction



**Figure (2.1): Scanning Electron Microscopy (SEM) Energy Disperse X-ray EDX (JEOL 7000f)**

#### 2.4.4 Fourier Transforms Infrared Spectroscopy Measurement

Figure (2.11), is Figure is a technique which is used to obtain an infrared spectrum of absorption or emission of a solid, liquid or gas. An FTIR spectrometer simultaneously collects high spectral resolution data over a wide spectral range. This confers a significant advantage over a dispersive spectrometer which measures intensity over a narrow range of wavelengths at a time. Fourier transform infrared spectra of xerogel, ZnO and Ni/ZnO samples were obtained in a FTIR-8400S spectrometer at room temperature in the  $4000 - 400 \text{ cm}^{-1}$  wavenumber range, with a  $4 \text{ cm}^{-1}$  resolution. Before each analysis, a pellet made of a mixture of specimens powder and KBr were pressed and dried overnight at  $105\text{C}^{\circ}$ .



**Figure (2.2): Fourier Transforms Infrared Spectrophotometer FTIR-8400S**

#### 2.4.5 UV. Measurement

The photoluminescence PL (Figure 2.2.4) spectroscopy is a powerful technique for the investigation and characterization of the optical properties of nanomaterials. The basic principle of the PL measurements is that, the ZnO semiconductor is excited by photon which has higher energy than the band gap of the ZnO. Then the incident photon is absorbed and create electron-hole pairs in the semiconductor. Within a short period of time the electron hole pairs are recombined and emit

photon from the semiconductor, the energy of the emitted photons reflects the carrier energy in the semiconductor. Finally, the emitted luminescence (light) and intensity are collected and recorded to generate a PL spectrum. A Perkin Elmer LS55 luminescence spectrofluorimeter was used to study spectra of fluorescence. The apparatus were operated at room temperature and the excitation source is a special Xenon flash tube that produces an intense short duration pulse of radiation over the spectral range. Excitation wavelength was at 465 nm.

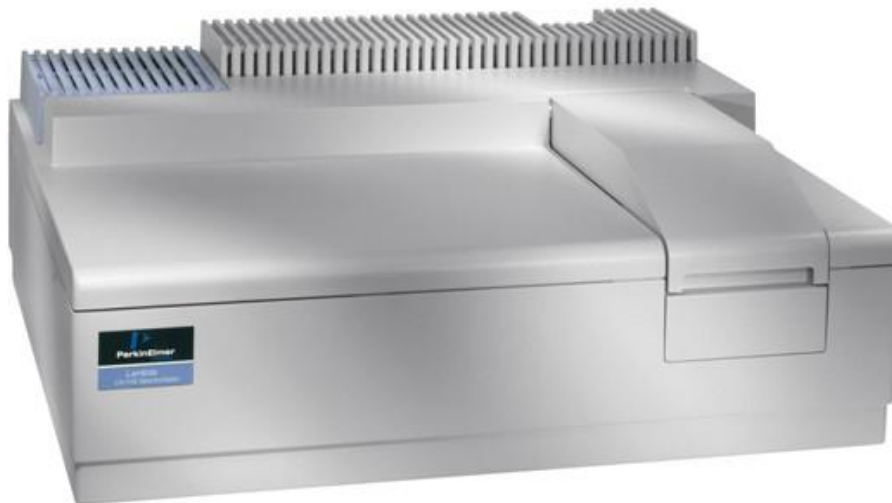


**Figure (2.3): Photoluminescence Analyzer PL (Perkin Elmer LS55 luminescence)**

#### **2.4.6 Methyl orange degradation kinetic**

Kinetics adsorption were studied using 1000 ml of Methyl orange solution with initial concentration of 5 mg/L and 5 mg of solid ware added and stirred in dark. A sample was withdrawn, as attached (table 3.1), residual concentration measured by spectrophotometer Labomed – UVS-2800 at maximum wavelength of 465 nm. The quantity of Methyl orange adsorbed per gram of catalysts at time (min) can be calculated by the following equation

$$q_t = \frac{(C_0 - C_t)V}{m}$$

Where  $q_t$  represents the quantity of adsorbed Methyl orange per gram of adsorbent (catalysts) at time,  $C_0$  is the initial Methyl orange concentration,  $C_t$  the concentration of Methyl orange at time  $t$ ,  $V$  is the volume of the Methyl orange solution (ml) and  $m$  represents the mass(mg) of the solid used. (Modwi et al, 2017).



**Figure (2.4): Spectrophotometer (Labomed – UVS-2800)**

## Chapter Three

### Results and Discussion

#### 3.1 Characterization of ZnO and Ni/ZnO nanoparticles

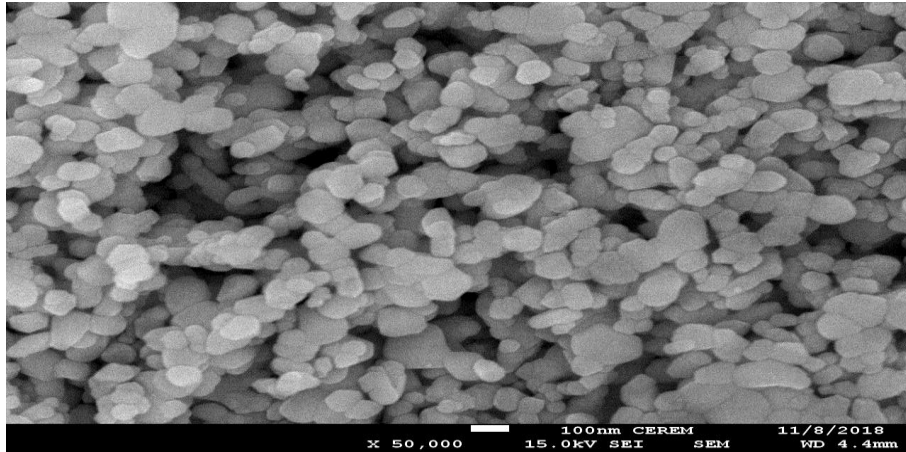
##### 3.1.1 Scanning electronic microscopic (SEM)

Fig (3.1) and (3.2) show the SEM image of pure ZnO and Ni/ZnO at 700 C°it is clear that the nanoparticles are spherical and slightly tangled for, both Ni/ZnO and ZnO with average particle size 62.45nm and 83.16nm for pure zinc oxide and nickel doped zinc oxide respectively in figure (3.2) and fig (3.4).



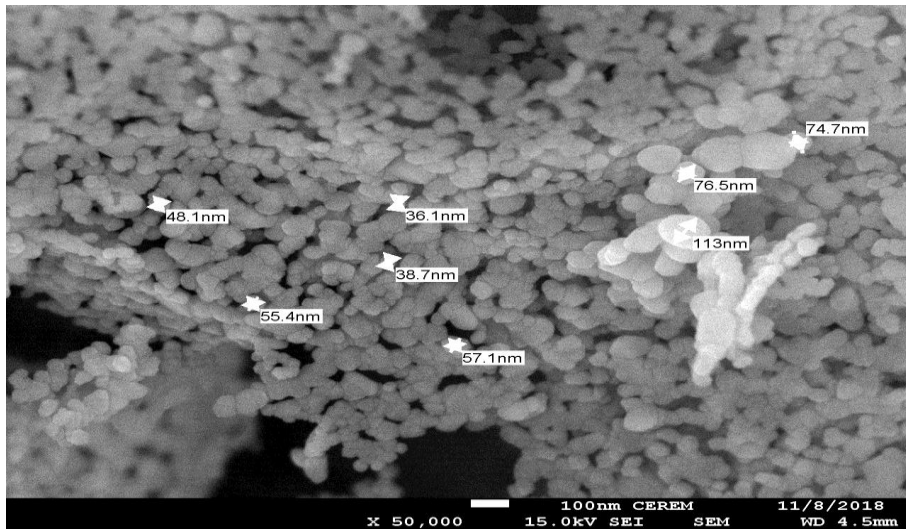
ZnO nanoparticeles

Figure (3.1): SEM Images of Pure ZnO



**Ni 5% doped ZnO nanoparticles**

**Figure (3.2) SEM Images of Ni 5% Doped ZnO**



**ZnO nanoparticles**

**Figure (3.3): SEM Images of Pure ZnO With Particle Size**

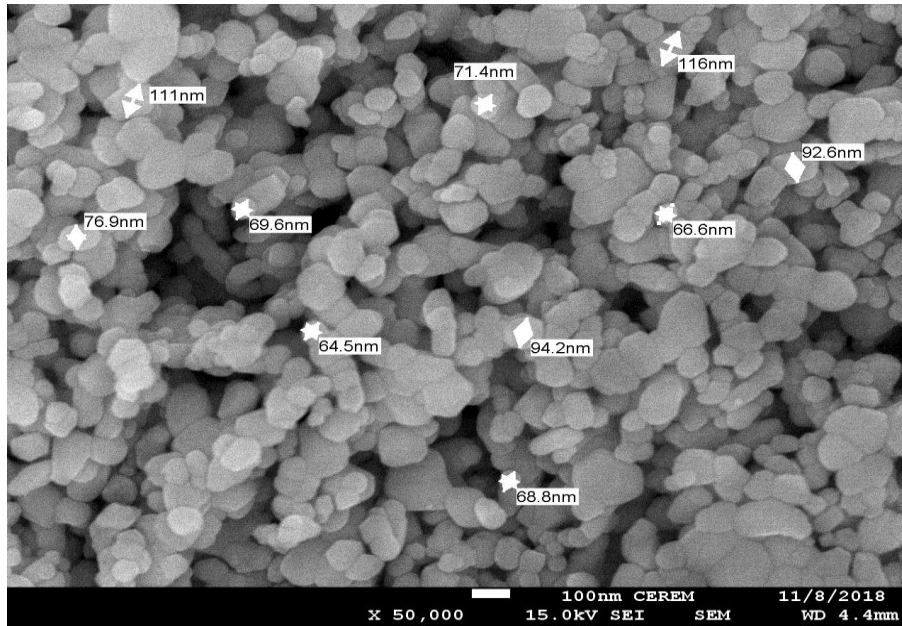


**Figure (3.4) Ni <sub>5%</sub> Doped ZnO Nanoparticles With Particle Size**

### **3.1.2 Fourier transforms infrared studies (FTIR)**

The chemical bonding and formation of wurtzite structure in ZnO (pure) and nickel doped ZnO were confirmed by FTIR measurements at room temperature. The spectra are shown in Fig (3.5) the broad absorption band at 3439.39, 1077.74, 3446.53 and 1075.74  $\text{cm}^{-1}$  can be attributed to the normal polymeric O-H stretching vibration and definition of H<sub>2</sub>O, respectively in ZnO and nickel doped ZnO lattices. Other sharp peaks observed at 1621.45 and 1615.60  $\text{cm}^{-1}$  can be attributed to H-O-H bending vibration, which in turn can be assigned to the small amount of H<sub>2</sub>O in the ZnO and nickel doped ZnO nano crystals. The absorption band observed between 2300 and 2400  $\text{cm}^{-1}$  are due to the existence of CO<sub>2</sub> molecule in the air . The vibration band at 446.31  $\text{cm}^{-1}$  assigned to the stretching mode of pure ZnO, shifted to a lower frequency at 438.48  $\text{cm}^{-1}$  for nickel doped ZnO. Hence, it suggested that Ni-ion was successfully, substituted into the crystal lattice of ZnO, which is in good agreement with (Modwi. A, et al, 2016)

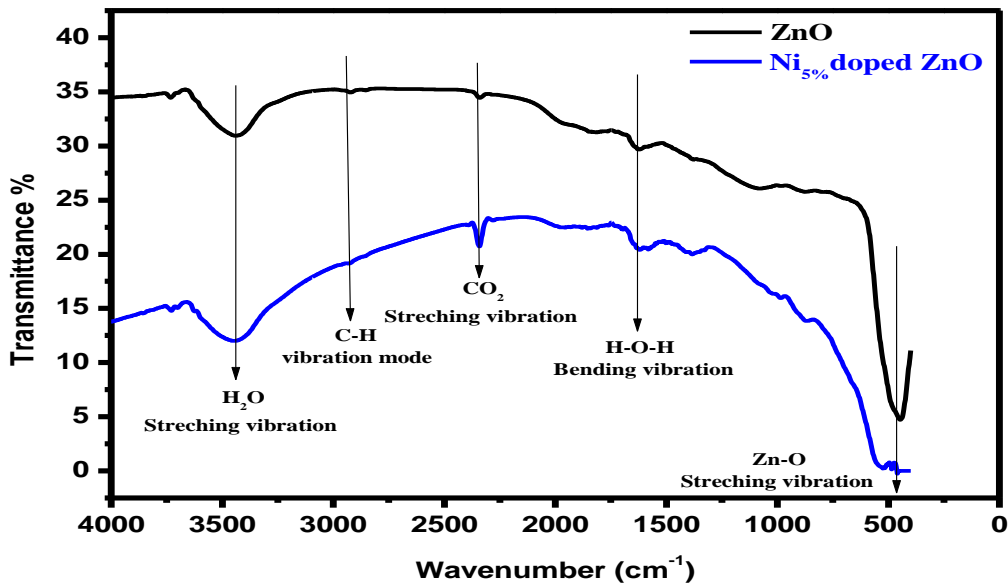


Figure (3.5)

### Fourier Transforms Infrared for ZnO and Ni /ZnO

### 3.2 Estimation of Band gap in ZnO and Ni /ZnO

ZnO and Ni/ZnO in UV-Vis range of the electromagnetic spectra, is shown fig (3.6) and (3.7) where a maxima is shown at 270nm and 275 nm for both respectively From the UV-Vis absorption data the band gap of ZnO and, Ni/ZnO was calculated using the relation (S.K., et al (2009)

$$(\alpha h\nu)^2 = c (h\nu - E_g) \quad (1)$$

$$\alpha = B (h\nu - E_g)^{-1/2}$$

$$(\alpha h\nu)^2 = c (h\nu - E_g)$$

Where c is constant. By plotting  $(\alpha h\nu)^2$  vs photon energy (hν) and extrapolating the straight line portion of the curve to interpret the abscissa fig(3.8),fig(3.9) , the value of the energy band gap is found to be (3.9eV) and 3.85eV for ZnO and Ni/ZnO respectively.

The increase of the band gap may be due to presence of impurities in the sample or elements Which release electron (Modwi et al, 2016).

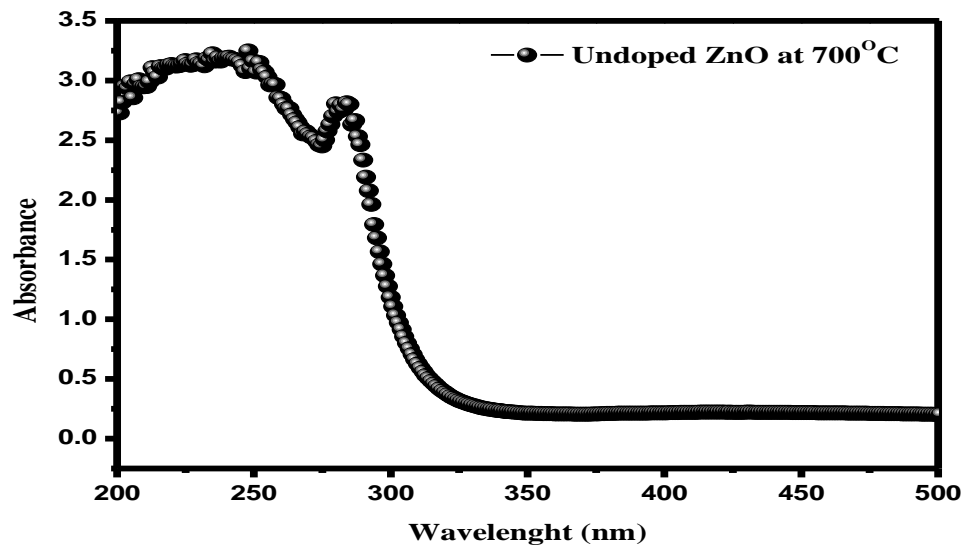


Figure (3.6)  
Undoped ZnO at 700 C°

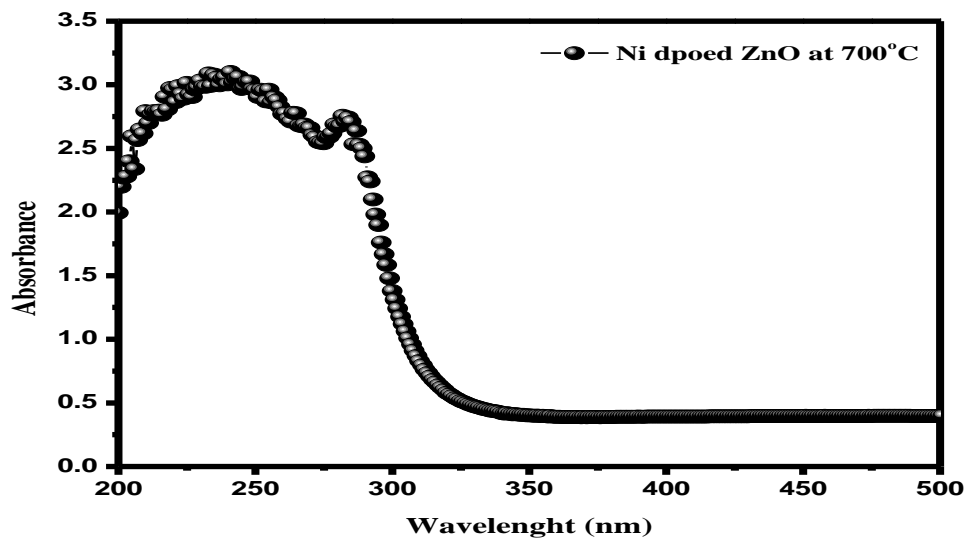


Figure (3.7)  
Ni doped ZnO at 700 C°

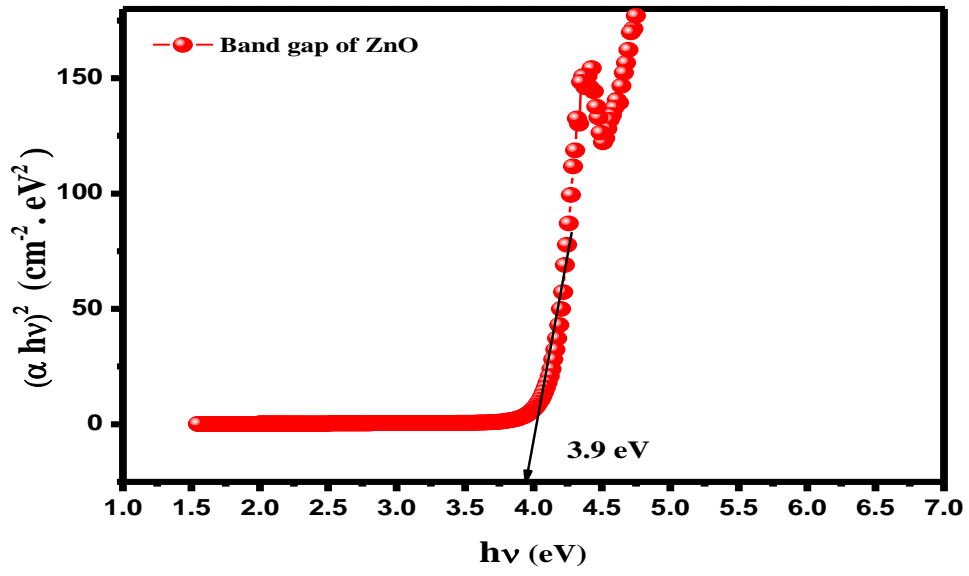


Figure (3.8) Band Gap of Pure ZnO

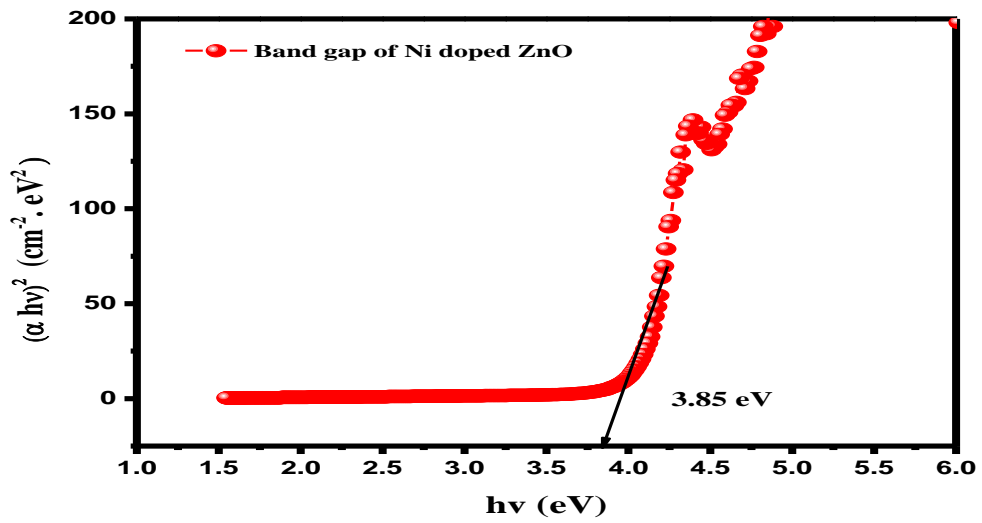


Figure (3.9) Band Gap of Ni/ZnO

### 3.3 Photo Catalytic Performance

#### 3.3.1 Kinetic Adsorption of Methyl orange

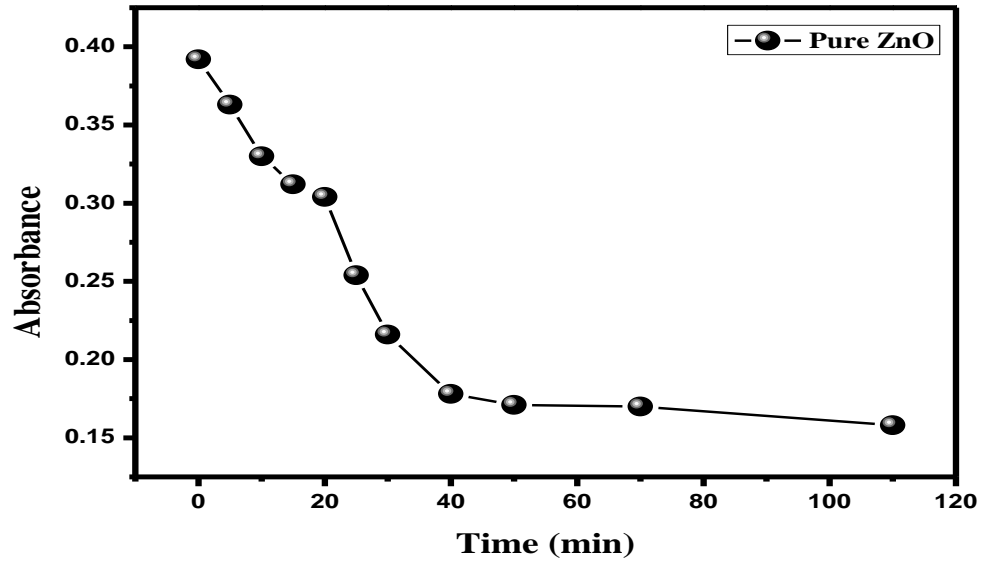
Table (3.1) and (3.2) show adsorption kinetic data for ZnO and Ni/ZnO nanoparticles Figure (3.10) and (3.12) show the variation of adsorption and Fig (3.11) (3.13) show plot of  $\text{Lin}(C_0/C_t)$  vs time for ZnO and Ni/ZnO nanoparticles, it is possible to calculate that the rate constant for photo degradation of methyl orange was 0.0185 and 0.0225 for ZnO and Ni/ZnO respectively.

Time	absorption	$\text{Lin}(C_0/C_t)$	Degradation efficiency %
0	0.392	0	0%
5	0.363	0.7686	7.4%
10	0.330	0.17217	15.8%
15	0.312	0.22826	20.4%
20	0.304	0.25423	22.5%
25	0.254	0.43393	35.2%
30	0.216	0.59598	44.9%
40	0.178	0.78948	54.6%
50	0.171	0.8296	56.4%
70	0.170	0.83546	56.6%
110	0.158	0.90867	60%

**Table (3.1)**  
**Adsorption Kinetic Data for Methyl Orange Using ZnO**

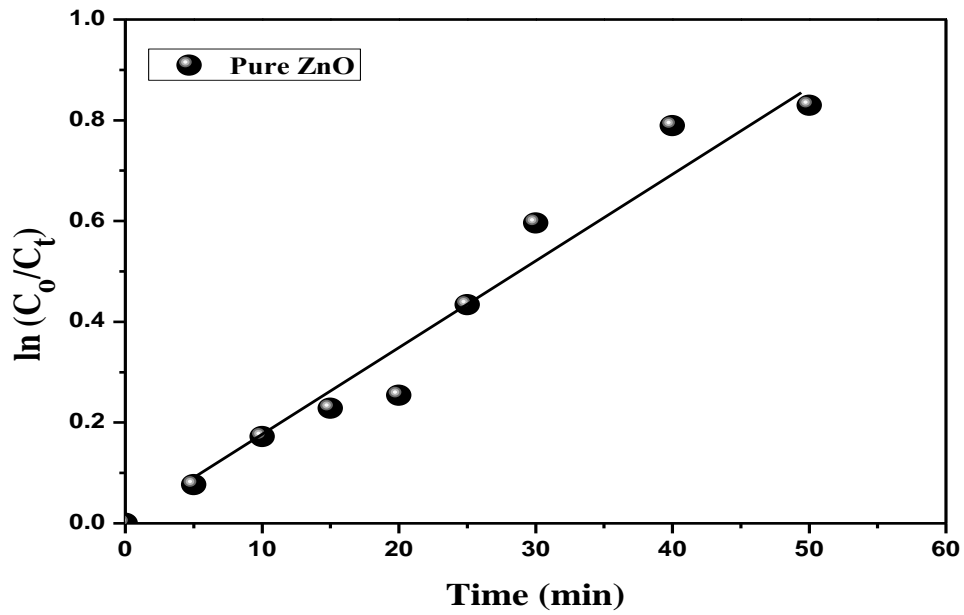
time	absorption	$\text{Lin}(C_0/C_t)$	Degradation efficiency %
0	0.392	0	0%
5	0.361	0.08238	8%
10	0.322	0.19671	18%
15	0.300	0.26748	23.5%
20	0.264	0.28768	32.7%
25	0.240	0.49062	38.8%
30	0.200	0.67294	49%
40	0.160	0.89609	59.2%
50	0.145	0.99453	63%
70	0.135	1.06599	65.6%
110	0.111	1.26173	71.7%

**Table (3.2)**  
**Kinetic Adsorption for Methyl Orange Using Ni/ZnO Nanoparticle**



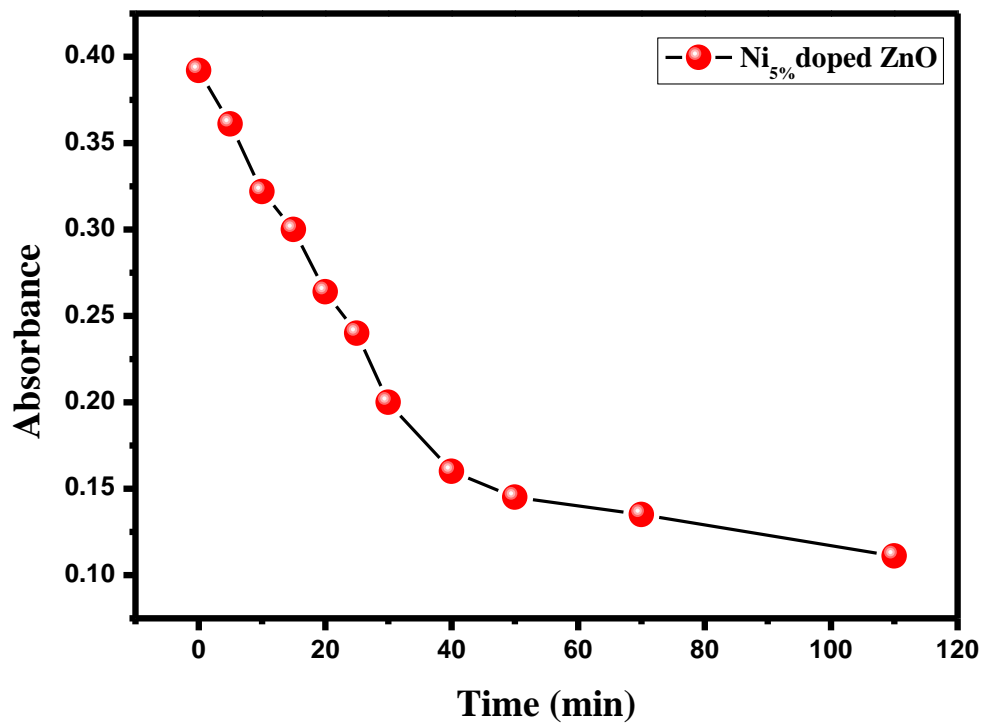
ZnO (Rate of photo degradation  $k=0.0185$ )

Figure (3.10): Absorbance VS Time



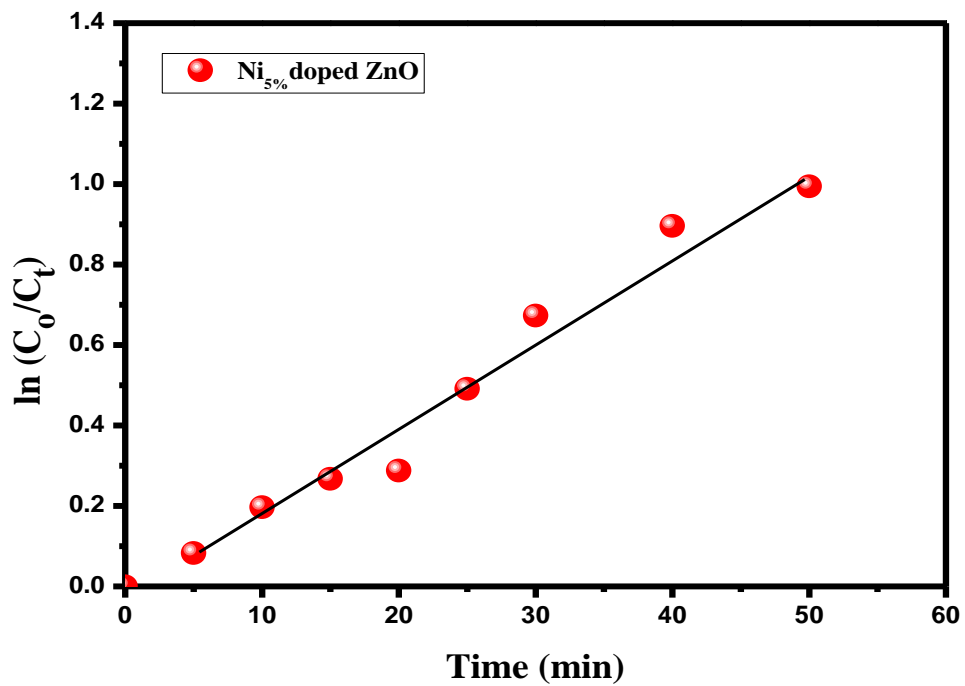
ZnO (Rate of photo degradation  $k=0.0185$ )

Figure (3.11)  $\ln C_0/C_t$  VS Time



Ni<sub>5%</sub> doped ZnO (Rate of photo degradation  $k=0.0225$ )

Figure (3.12) Absorbance VS Time



Ni<sub>5%</sub> doped ZnO (Rate of photo degradation  $k=0.0225$ )

Figure (3.13): lnC<sub>0</sub>/C<sub>t</sub> VS Time

### 3.3.2 Catalytic Degradation

The photoactivity performance of ZnO and Ni/ZnO specimens were evaluated using (methyl orange) dye as a pollutant under U.V irradiation.

The irradiation source was a Philips HPK 125W lamp (365). For UV degradation. The concentration of methyl orange was (initial concentration 0.392), while that of the different photocatalysts was 0.158 and 0.111 after 110 min for both pure zinc oxide and nickel doped zinc oxide respectively.

After achieving adsorption equilibrium in the dark, the solution was illuminated for the photocatalytic kinetic study.

A sample of the methyl orange solution was withdrawn every as attached in table(3.1),and the table (3.2).

Residual concentration were measured by UV-vis spectroscopy at a wavelength  $\lambda_{max}= 465nm..$

The photocatalytic degradation efficiency was calculated using the following equation.

$$\% \text{ degradation} = \frac{(C_0 - C_t)}{C_0} * 100$$

Where  $C_0$  and  $C_t$  are methyl orange initial concentration (fixed at 0.392) and

Time t concentration, respectively. (Modwi. A, et al, 2016)

Table (3.1) and table (3.2). degradation after 110 min for pure zinc oxide was 60% and 71.7% for nickel doped zinc oxide that is clear the doping of nickel ion to zinc oxide enhance the efficiency than pure zinc oxide .

## Conclusions

- Synthesis of zinc oxide and nickel doped zinc oxide was carried out and the nano particles formed were characterized by SEM, FTIR
- The band gap of ZnO and Ni/ZnO nanoparticles were calculated using Tauc equation and found to be 3.9, 3.85eV for ZnO and Ni/ZnO respectively
- The Ni-doped ZnO nano catalyst was more efficient compared to pure ZnO nano catalyst where the percentage of photo degradation of methyl orange was enhanced by factor of (1:1.2) for pure ZnO and Ni/ZnO respectively
- The rate constant of catalytic photo degradation is 18% less for ZnO

## References

- Ali S.M.U., Member S., Ieee, Muhammad H. Asif, Fulati A., Nur O., Willander M., Br''anmark C., Stralfors P., Ulrika H. Englund, Elinder, and Danielsson B., (2011), Interacellular  $K^+$  Determination With a potentiometric Microelectrode Based on ZnO Nanowires, *IEEE Transactions on Nanotechnology*, **10**:913-919.
- Ali, F.A.A.M., 2016. Synthesis and Characterization of Zinc Oxide Nanostructure at Low Temperature (*Doctoral dissertation, Sudan University of Science and Technology*).
- Amin G., Zaman S., Zainelabdin A., Nur O., and Willander M., (2010), Zinc Oxide nanorods polymer hybrid white light emitting diode grown on a disposal paper substrate, *Phys. Status Solidi RRL*, **5**, 2:71-73.
- Amin, G., 2012. ZnO and CuO nanostructures: low temperature growth, characterization, their optoelectronic and sensing applications (*Doctoral dissertation, Linköping University Electronic Press*).
- Anderson, P., He, X., Buehler, C., Teney, D., Johnson, M., Gould, S. and Zhang, L., 2018. Bottom-up and top-down attention for image captioning and visual question answering. *In Proceedings of the IEEE conference on computer vision and pattern recognition* (pp. 6077-6086).
- Asif M.H., Ali S.M.U., Nur O., Willander M., Englund U.H., Elinder F., (2010), Functionalized ZnO nanorod-based selective magnesium ion sensor for intracellular measurement, *Biosensors and Bioelectronics*, **26**:1118-1123.
- Baghbanzadeh, M., Carbone, L., Cozzoli, P.D. and Kappe, C.O., 2011. Microwave assisted synthesis of colloidal inorganic nanocrystals. *Angewandte Chemie International Edition*, **50**(48), pp.11312-11359.
- Baláž, P., Achimovičová, M., Baláž, M., Billik, P., Cherkezova-Zheleva, Z., Criado, J.M., Delogu, F., Dutková, E., Gaffet, E., Gotor, F.J. and Kumar, R., 2013. Hallmarks of mechanochemistry: from nanoparticles to technology. *Chemical Society Reviews*, **42**(18), pp.7571-7637.
- Baruah S. and Dutta J., (2009), hydrothermal growth of ZnO Nanostructures, *science and technology of advanced material*, **10**:1-18.
- Bora, T., Sathe, P., Laxman, K., Dobretsov, S. and Dutta, J., 2017. Defect engineered visible light active ZnO nanorods for photocatalytic treatment of water. *Catalysis Today*, **284**, pp.11-18.
- Dinh C.T., Nguyen T.D. Kleitz F., and Dot.O. (2012), - Shape- Controlled Synthesis of Metal Oxide Nanocrystal, *Controlled Nanofabrication's: Advances and Application*, 328-367.

Dupas, C. and Lahmani, M. eds., 2007. Nanoscience: Nanotechnologies and nanophysics. Springer Science & Business Media.

Eatemadi, A., Daraee, H., Karimkhanloo, H., Kouhi, M., Zarghami, N., Akbarzadeh, A., Abasi, M., Hanifehpour, Y. and Joo, S.W., 2014. Carbon nanotubes: properties, synthesis, purification, and medical applications. *Nanoscale research letters*, **9(1)**, p.393.

Geng, L.J.P.X.J. and Che, B.Q.F.D.Y., 2009. Applications of Nanotechnology in Capillary Electrophoresis and Microfluidic Chip Electrophoresis Biomolecular Separations. *Progress In Chemistry*, **21(09)**, p.1905.

Gomez, J.L. and Tigli, O., 2013. Zinc oxide nanostructures: from growth to application. *Journal of Materials Science*, **48(2)**, pp.612-624.

Goodman, E.D., Schwalbe, J.A. and Cargnello, M., 2017. Mechanistic understanding and the rational design of sinter-resistant heterogeneous catalysts. *ACS Catalysis*, **7(10)**, pp.7156-7173.

Israr.Q., Sadafj.R., M.H. Nur O., Willander M,Danielsson B,(2010),Potentiometric cholesterol biosensor based on ZnO nanorods chemically grow on agwire,Thin Solid Films,**519**:1106-1109.

Jiang, H., 2011. Chemical preparation of graphene based nanomaterials and their applications in chemical and biological sensors. *Small*, **7(17)**, pp.2413-2427.

Jun, Y.W., Choi, J.S. and Cheon, J., 2006. Shape control of semiconductor and metal oxide nanocrystals through nonhydrolytic colloidal routes. *Angewandte Chemie International Edition*, **45(21)**, pp.3414-3439.

Kishwar S.,Asif M.H.,Nur O., Willander M., Larsson P-O,(2010),-Intracellular ZnO Nanorods Conjugated with Protoporphyrin for Local Mediated Photochemistry and Efficient Treatment of Single Cancer Cell,Springer,**5**:1669-1674.

Koch, C.C., 2009. Nanostructured materials: an overview. *Bulk Nanostructured Materials*, pp.1-20.

Kolodziejczak-Radzimska A. and Jesionows T., (2014), Zinc Oxide-From Synthesis to Application, m, material, **7**:2831-2881.

Kołodziejczak-Radzimska, A. and Jesionowski, T., 2014. Zinc oxide—from synthesis to application: a review. *Materials*, **7(4)**, pp.2833-2881.

Kołodziejczak-Radzimska, A. and Jesionowski, T., 2014. Zinc oxide—from synthesis to application: a review. *Materials*, **7(4)**, pp.2833-2881.

Koziej, D., Lauria, A. and Niederberger, M., 2014. 25th anniversary article: metal oxide particles in materials science: addressing all length scales. *Advanced materials*, **26(2)**, pp.235-257.

- Kumar H., Rani R., (2013), Structural and Optical Characterization of ZnO Nanoparticles Synthesized by Microemulsions Route, *International Letters of Chemistry , Physics and Astronomy*, **14**:26-36.
- Kumar, H. and Rani, R., 2013. Structural and optical characterization of ZnO nanoparticles synthesized by microemulsion route. *International Letters of Chemistry, Physics and Astronomy*, **14**, pp.26-36.
- Lanje, A.S., Sharma, S.J., Ningthoujam, R.S., Ahn, J.S. and Pode, R.B., 2013. Low temperature dielectric studies of zinc oxide (ZnO) nanoparticles prepared by precipitation method. *Advanced Powder Technology*, **24(1)**, pp.331-335.
- Li, L., Zhai, T., Bando, Y. and Golberg, D., 2012. Recent progress of one-dimensional ZnO nanostructured solar cells. *Nano Energy*, **1(1)**, pp.91-106.
- Loidreau, Y. and Besson, T., 2011. Microwave-assisted thermal decomposition of formamide: a tool for coupling a pyrimidine ring with an aromatic partner. *Tetrahedron*, **67(26)**, pp.4852-4857.
- Mahamuni, P.P., Patil, P.M., Dhanavade, M.J., Badiger, M.V., Shadija, P.G., Lokhande, A.C. and Bohara, R.A., 2019. Synthesis and characterization of zinc oxide nanoparticles by using polyol chemistry for their antimicrobial and antibiofilm activity. *Biochemistry and biophysics reports*, **17**, pp.71-80.
- Modwi.A,Abbo.M.A,Hassan.E.A,Al-Duaij.O.K,Houas.A,(2017),Adsorption Kinetics and photo catalytic degradation of malachite green (MG) via Cu/ZnO nanocomposites,*Journal of Environmental Chemical Engineering*,**5**,5954-5960
- Modwi.A,Hassan.E.A,Abbo.M.A,Houas.A,(2016)Effect of annealing on physicochemical and photo catalytic activity of Cu5% loading on ZnO synthesized by sol-gel method, *Journal of Environmental Chemical Engineering*,**12**,59-66
- Moloantoa, R.J., 2016. Studies of structural and optical variations of nanosized TiO<sub>2</sub> introduced by precious metal dopants (Au, Pt, Pd and Ag) (Doctoral dissertation, University of Limpopo).
- Pal S.I., jan., Manna P.K., Mohanta G.P., Manavalan R., (2011), An overview of preparation and characterization, *Journal of Applied pharmaceutical Science*, **1 (6)**: 228-234.
- Pal, S.L., Jana, U., Manna, P.K., Mohanta, G.P. and Manavalan, R., 2011. Nanoparticle: An overview of preparation and characterization. *Journal of applied pharmaceutical science*, **1(6)**, pp.228-234.
- Pattison, D.I., Rahmanto, A.S. and Davies, M.J., 2012. Photo-oxidation of proteins. *Photochemical & Photobiological Sciences*, **11(1)**, pp.38-53.

- Prof. Dr. Klingshirn C., (2007), ZnO: Material, physics and Application, *ChemPhysChem*, **8**:782-803.
- Reddy, P.S., Ramaswamy, P. and Sunanda, C., 2010. Role of gold nanoparticles in early detection of oral cancer. *Journal of Indian Academy of Oral Medicine and Radiology*, **22**(1), p.30.
- Roberson, M., Rangari, V., Jeelani, S., Samuel, T. and Yates, C., 2014. Synthesis and characterization silver, zinc oxide and hybrid silver/zinc oxide nanoparticles for antimicrobial applications. *Nano Life*, **4**(01), p.1440003.
- Roco, M.C., Mirkin, C.A. and Hersam, M.C., 2011. Nanotechnology research directions for societal needs in 2020: summary of international study.
- S. K. Mehta, Sanjay Kumar, Savita Chaudhary and K. K. Bhasin, (2009), Nucleation and growth of surfactant passivated CdS and HgS NPs: Time dependent Absorption and Luminescence profiles, Pinjab University, (Supplementary Material (ESI) for *Nanoscale*, P.1.
- Sapkota A., Anceno A.J, Baruah S, Shipino. Vand Dutta J., (2011), Zinc Oxide nanorod mediated visible light photo inactivation of model microbes in water, *nanotechnology*, **22**:1-7.
- Sau, T.K. and Rogach, A.L., 2010. Nonspherical noble metal nanoparticles: colloid chemical synthesis and morphology control. *Advanced Materials*, **22**(16), pp.1781-1804.
- Tao, A.R., Habas, S. and Yang, P., 2008. Shape control of colloidal metal nanocrystals. *small*, **4**(3), pp.310-325.
- Tiruwa, R., 2016. A review on nanoparticles—preparation and evaluation parameters. *Indian journal of pharmaceutical and biological research*, **4**(2), pp.27-31.
- Umar A. and Hahn Y-B., (2010), Metal Oxide Nanostructures and Their Application, Aaseem-M., Umar A. and Hajn y-B., ZnO Nanoparticles :Growth, Properties , and Application, American Scientific Publishers, **5**:1-36.
- Vaseem, M., Umar, A. and Hahn, Y.B., 2010. ZnO nanoparticles: growth, properties, and applications. *Metal oxide nanostructures and their applications*, **5**(1).
- Vayssieres L., Keis K., Lindquist S-E, and Hagfeldt A., (2001), Purpose-Built Anisotropic Metal Oxide Material : 3D Highly Oriented Microrod Array of ZnO, *J.Phys.Chem*, **105**:3350-3352.
- Vayssieres, L., Keis, K., Lindquist, S.E. and Hagfeldt, A., 2001. Purpose-built anisotropic metal oxide material: 3D highly oriented microrod array of ZnO. *The Journal of Physical Chemistry B*, **105**(17), pp.3350-3352.
- Wang, Z.L., 2004. Zinc oxide nanostructures: growth, properties and applications. *Journal of physics: condensed matter*, **16**(25), p.R829.

Wang, Z.L., 2009. ZnO nanowire and nanobelt platform for nanotechnology. *Materials Science and Engineering: R: Reports*, **64(3-4)**, pp.33-71.

Willander M., UI Hassan K., Nur O., Zainelabdin A., Zaman S. and Amin G., (2012), Recent progress on growth and device development of ZnO and CuO nanostructure and graphene nanosheets, *Journal of Material Chemistry*, **22**:2337-2350.

Willander M., Nur O., Fakhar-e-Alam M., Sadaf J.R, Israr M.Q, Sultana K., Ali S.M.U, Asif M.H, (2011), Application of Zinc Oxide Nanowires for Bio-photonics and Bio-electronic, *Oxide-based Materials and Devices* **7940**: 1-13.

Zainelabdin A., Zaman S., Amin G., Nur O., and Willander M., (2010), Deposition of Well-Aligned ZnO Nanorods at 50°C on Metal, Semiconducting Polymer, and Copper Oxides Substrates and Their Structural and Optical Properties, *Crystal Growth & Design*, **10**:3250-3256.

Zainelabdin A., Amin G., Zaman S., Nur O., Lu, J. Hultman L, and Willander M., (2012), CuO/ZnO nanocorals synthesis via hydrothermal technique: growth mechanism and their application as Humidity Sensor, *Journal of Materials Chemistry*, **22**:11583-11590.

Zainelabdin, A., Zaman, S., Amin, G., Nur, O. and Willander, M., 2010. Deposition of well-aligned ZnO nanorods at 50 C on metal, semiconducting polymer, and copper oxides substrates and their structural and optical properties. *Crystal Growth & Design*, **10(7)**, pp.3250-3256.

Zhang, Y.P., Yang, J.H., Li, L.L., Cui, C.X., Li, Y., Liu, S.Q., Zhou, X.M. and Qu, L.B., 2019. Facile fabrication of superhydrophobic copper-foam and electrospinning polystyrene fiber for combinational oil–water separation. *Polymers*, **11(1)**, p.97.